



Titre: A hybrid numerical-semi-analytical method for computer simulations of groundwater flow and heat transfer in geothermal borehole fields
Title:

Auteurs: Massimo Cimmino, & Bantwal Rabi Baliga
Authors:

Date: 2019

Type: Article de revue / Article

Référence: Cimmino, M., & Baliga, B. R. (2019). A hybrid numerical-semi-analytical method for computer simulations of groundwater flow and heat transfer in geothermal borehole fields. *International Journal of Thermal Sciences*, 142, 366-378.
Citation: <https://doi.org/10.1016/j.ijthermalsci.2019.04.012>

 **Document en libre accès dans PolyPublie**
Open Access document in PolyPublie

URL de PolyPublie: <https://publications.polymtl.ca/5502/>
PolyPublie URL:

Version: Version finale avant publication / Accepted version
Révisé par les pairs / Refereed

Conditions d'utilisation: CC BY-NC-ND
Terms of Use:

 **Document publié chez l'éditeur officiel**
Document issued by the official publisher

Titre de la revue: International Journal of Thermal Sciences (vol. 142)
Journal Title:

Maison d'édition: Elsevier
Publisher:

URL officiel: <https://doi.org/10.1016/j.ijthermalsci.2019.04.012>
Official URL:

Mention légale: © 2019. This is the author's version of an article that appeared in *International Journal of Thermal Sciences* (vol. 142). The final published version is available at <https://doi.org/10.1016/j.ijthermalsci.2019.04.012>. This manuscript version is made available under the CC-BY-NC-ND 4.0 license <https://creativecommons.org/licenses/by-nc-nd/4.0/>
Legal notice:

A hybrid numerical-semi-analytical method for computer simulations of groundwater flow and heat transfer in geothermal borehole fields

Massimo Cimmino^{a§}, Bantwal R. (Rabi) Baliga^b

^aÉcole Polytechnique de Montréal, Département de génie mécanique

Case Postale 6079, succursale “centre-ville”, Montréal, Québec, Canada H3C 3A7

[§]Corresponding author: massimo.cimmino@polymtl.ca

^bDepartment of Mechanical Engineering, McGill University

817 Sherbrooke St. W., Montreal, Quebec H3A 0C3, Canada

A hybrid numerical-semi-analytical method for computer simulations of groundwater flow and heat transfer in geothermal borehole fields

Abstract

The formulation of a hybrid numerical-semi-analytical method for cost-effective simulations of heat transfer in fields of vertical geothermal boreholes, in the presence of groundwater flow, is presented. An amalgamation of a co-located control-volume finite element method and a finite volume method is used to solve 1) a volume-averaged continuity and the Darcy-Brinkman-Frochheimer equations to obtain the distribution of the groundwater flow; and 2) an unsteady three-dimensional volume-averaged advection-conduction equation to calculate the related ground temperature distribution, assuming local thermodynamic equilibrium between the groundwater and the soil particles. The bulk temperature distribution of the working fluid (flowing inside the legs of a U-tube pipe inserted inside each borehole and kept in place by grout) and the related heat extraction (or addition) rate are obtained using a semi-analytical method to solve a quasi-steady quasi-one-dimensional model. The conditions of no-slip, impermeability, equality of temperature, and continuity of heat flux are used at the interface between each borehole and the groundwater-saturated soil in the borehole field. The proposed method is applied to test and demonstration problems to demonstrate its capabilities.

Key words: Geothermal borehole fields; groundwater flow; hybrid numerical-semi-analytical method; Darcy-Brinkman-Forchheimer equations; volume-averaged advection-conduction equation; control-volume finite element method

1. Introduction

Geothermal systems are playing an increasingly important role in ongoing worldwide efforts to develop environmentally friendly, sustainable, and efficient ways of fulfilling space heating and cooling demands. A promising approach in this regard is based on ground-source heat pumps (GSHPs) coupled to vertical geothermal boreholes (hereafter referred to as boreholes in this paper) [Spitler (2005); Kavanaugh and Rafferty (2014)]. Designing of GSHPs is facilitated by accurate predictions of the working-fluid and ground temperatures, and the related heat extraction and injection rates, during their operation. The techniques used for such predictions are often based on mathematical models that invoke the assumption of purely conductive heat transfer in the ground that surrounds the boreholes [Yang et al. (2010); Li and Lai (2015)]. However, if the flow of groundwater in a borehole field is sufficiently high, it could have a significant effect on the temperatures of the ground and the boreholes, and the related heat transfer rates, as discussed by Chiasson et al. (2000), Fan et al. (2007), Wang et al. (2009), Chiasson and O'Connell (2011), Zanchini et al. (2012), Capozza et al. (2013), Hecht-Méndez et al. (2013), and Choi et al. (2013), for example.

Accounting for the effects of groundwater flow has also resulted in several improvements to the analyses of geothermal thermal-response tests and the data deduced from them, as demonstrated, for example, by the works of Gehlin and Hellström (2003), Lee and Lam (2012), Therrien et al. (2010), Raymond et al. (2011), Wagner et al. (2013), Rouleau and Gosselin (2016), Rouleau et al. (2016), and Zhang et al. (2016). It should also be noted that the heterogeneity of the soil hydraulic conductivity and the mixing of flowing groundwater at the pore scale, could create disparities between the longitudinal (parallel to the direction of groundwater flow) and the transverse (perpendicular to the direction of groundwater flow)

dispersion of heat, as discussed, for example, in the works of Hsu and Cheng (1990), Metzger et al. (2004), Hidalgo et al. (2009), Hecht-Méndez et al. (2010), Diersch et al. (2011a; 2011b), Molina-Giraldo et al. (2011a), Chiasson and O'Connell (2011), and Nield and Bejan (2013). Furthermore, in soils of sufficiently high hydraulic conductivity, buoyancy-driven natural convection can also affect the performance of geothermal systems, as shown, for example, in the works of Zhao et al. (2008) and Ghoreishi-Madiseh et al. (2013).

Analytical solutions to several simplified mathematical models of heat transfer in borehole fields with uniform groundwater flow have been proposed. They are based on adaptations and extensions of the seminal works of Carslaw and Jaeger (1959), Eskilson (1987), and Hellström (1991). These analytical approaches typically employ moving-infinite-line-source and moving-finite-line-source techniques, as illustrated, for example, in the works of Sutton et al. (2003), Diao et al. (2004), Molina-Giraldo et al. (2011b), Tye-Gingras and Gosselin (2014), and Rivera et al. (2015). Erol et al. (2015) have used a moving-finite-line-source model for investigating heat transfer in borehole fields with groundwater flow and different longitudinal and transverse thermal conductivities (to account for the effects of thermal dispersion).

Compared to analytical methods, such as those mentioned above, numerical methods offer enhanced accuracy in the simulation of heat transfer in borehole fields [Yang et al. (2010)]. Numerical simulations of unsteady heat transfer in borehole fields, without and with groundwater flow, and based on finite difference, spectral, unstructured finite volume, and finite element methods, are discussed, for example, in the works of Rottmayer et al. (1997), Yavuzturk et al. (1999), Li and Zheng (2009), Bauer et al. (2011), Al-Khoury and Focaccia (2016), and Dai et al. (2016). However, unsteady and fully multidimensional numerical simulations of the heat transfer processes in borehole fields, in both the ground and the boreholes, are quite expensive

computationally [Yang et al. (2010)]. Thus, for incorporation in design and energy-analysis procedures for borehole fields, hybrid numerical-analytical and numerical-semi-analytical methods, in which numerical simulations of heat transfer in the ground are coupled with approximate analytical or semi-analytical solutions of heat transfer in the boreholes (including the working fluid flowing through the U-tubes inserted in them), are an attractive cost-effective alternative (offering acceptable accuracy at affordable costs) to fully numerical and also completely analytical methods [Yang et al. (2010); Li and Zheng (2009); Bauer et al. (2011); Choi et al. (2013)].

In this paper, the formulation of a hybrid numerical-semi-analytical method for cost-effective simulations of heat transfer in borehole fields in the presence of groundwater flow is presented; it is then checked against a moving-finite-line-source analytical solution for a simplified version of the problem of interest; and, finally, its application to a demonstration problem and the results are discussed. In this method, an amalgamation of a co-located control-volume finite element method and a finite volume method (CVFEM and FVM) [Baliga and Atabaki (2006); Lamoureux and Baliga (2011)] is used to solve 1) a volume-averaged continuity equation and the Darcy-Brinkman-Frochheimer equations to obtain the distribution of the groundwater flow (assumed to be steady and two-dimensional in the horizontal cross-section of the borehole field); and 2) an unsteady three-dimensional volume-averaged advection-conduction equation to calculate the ground temperature distribution, assuming local thermodynamic equilibrium between the groundwater and the soil particles [Vafai (2005); Nield and Bejan (2013)]. The bulk temperature distribution of the working fluid (flowing inside the legs of a U-tube pipe inserted inside each borehole and kept in place by grout) and the heat extraction (or addition) rates are obtained using a semi-analytical solution to a quasi-steady

quasi-one-dimensional model, based on the concept of a delta-circuit of thermal resistances [Hellström (1991)].

The hybrid numerical-semi-analytical method proposed in this paper follows the works of Bernier and Baliga (1992) and Lamoureux and Baliga (2015), who proposed cost-effective hybrid methods for computer simulations of closed-loop thermosyphons, and Cotta and Mikhailov (2006). It also complements and extends the following two hybrid methods proposed for the investigation of heat transfer in borehole fields: 1) the method of Li and Zheng (2009), who used an unstructured cell-centered finite volume method for simulations of unsteady three-dimensional pure conduction heat transfer in the ground and a quasi-steady quasi-three-dimensional model [Yang et al. (2010)] for calculating the bulk temperature distribution of the working fluid; and 2) the method of Choi et al. (2013), who used a commercial finite element code (COMSOL Multiphysics 4.2a) to solve a two-dimensional steady version of the Darcy equation [Vafai (2005); Nield and Bejan (2013)] for the groundwater flow and a transient volume-averaged two-dimensional convection-conduction equation for heat transfer in the ground, and coupled these numerical solutions with an analytical solution of a model of the average (arithmetic mean) of the inlet and outlet bulk temperatures of the working fluid flowing through the U-tubes inserted in the boreholes.

2. Layout of the borehole field and related notation

Attention in this work is focused on vertical boreholes, each with a single U-tube pipe inserted symmetrically within it and held in place by grout. The vertical and horizontal cross sections of a borehole, n , are shown in Fig. 1. There are N_b such boreholes in the field of interest. Each of these boreholes has an active (or heated) length H and a radius r_b ; and the active length starts at

a depth D below the ground surface. The working (or heat carrier) fluid flows through each borehole at a mass flow rate of \dot{m}_f through a U-tube pipe of inner radius $r_{p,i}$ and outer radius $r_{p,o}$. The ground surface or top boundary of the borehole field is indicated by Γ_T , the interface between borehole n and the surrounding ground in the borehole field is denoted by $\Gamma_{b,n}$, and the vertical coordinate z starts at the ground surface and is directed downwards. The boreholes are evenly spaced on a square grid, with a distance B between adjacent boreholes, as indicated in Fig. 2 for a field of 3×2 boreholes. The east, west, north, and south boundaries of the borehole field (see Fig. 2) are denoted by Γ_E , Γ_W , Γ_N , and Γ_S , respectively; and the groundwater enters the borehole field with a uniform velocity, U_∞ , and temperature, T_g , across the full west boundary, Γ_W .

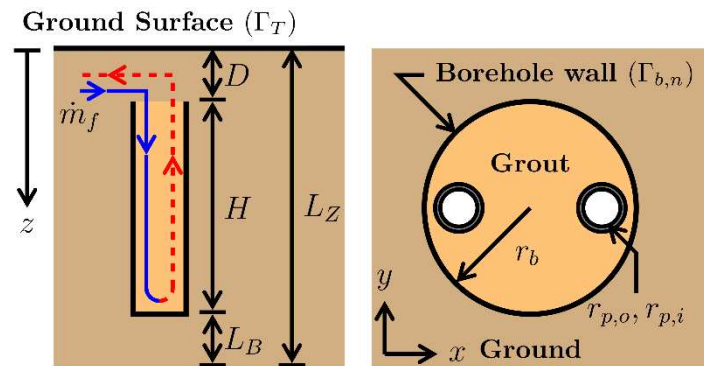


Figure 1. Schematic representations of the vertical (left) and horizontal (right) cross-sections of a borehole and the related notation

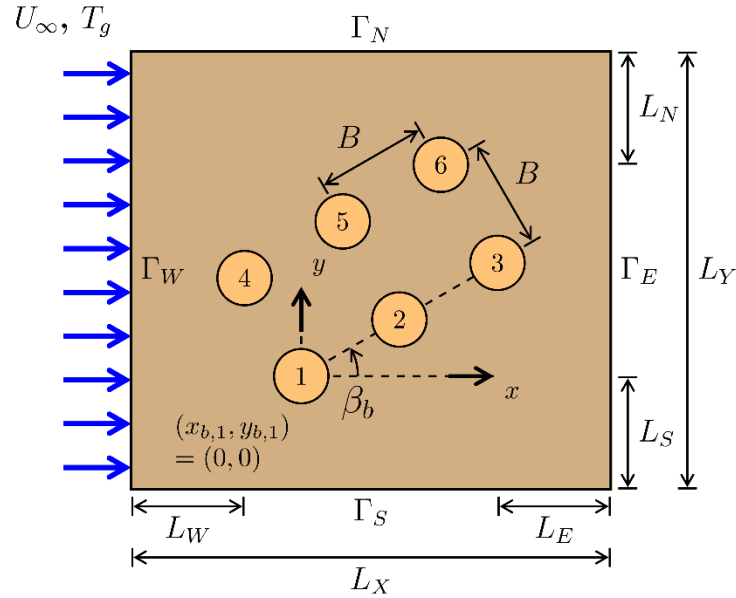


Figure 2. Schematic representation of a horizontal cross-section of the borehole field and the related notation

3. Mathematical models of groundwater flow, temperature distributions, and heat transfer in the borehole field

The assumptions invoked in these mathematical models are presented first in this section. Then the equations that were used to model the groundwater flow in the borehole field, the related temperature distribution and heat transfer in the groundwater-saturated soil, and the temperature distribution and heat transfer in each borehole, in that order, are presented.

3.1. Assumptions

The following assumptions are invoked in the mathematical models adopted in this work:

- The thermophysical properties of the dry soil in the borehole field, and also the grout and U-tube pipe wall in the boreholes, are uniform and constant
- The groundwater is an incompressible Newtonian fluid and its thermophysical properties are uniform and constant

- The soil in the borehole field is fully saturated with groundwater, and it has uniform and constant effective thermophysical properties
- On the entire west boundary (span and depth) of the borehole field, the groundwater velocity (magnitude and direction) and temperature (denoted by U_∞ and T_g , respectively, as shown in Fig. 2) are spatially uniform and invariant in time
- The groundwater-saturated soil in the borehole field is initially at a spatially uniform temperature T_g (or the initial geothermal gradient in the domain of interest is considered insignificant)
- The ground-surface ($z = 0$) temperature remains constant throughout and is equal to the initial undisturbed ground temperature T_g
- Buoyancy-driven natural convection is negligibly small, both in the groundwater and in the working fluid (flowing through the U-tube pipe in each of the boreholes)
- The groundwater flow is effectively steady and two-dimensional in the horizontal cross-section of the borehole field
- There is local thermodynamic equilibrium between the groundwater and the soil particles, thus the local intrinsic phase-average temperatures of the soil particles and the groundwater are effectively the same and governed by a single volume-average advection-conduction equation [Vafai (2005); Nield and Bejan (2013)]
- The viscous dissipation and the thermal dispersion due to groundwater movement are negligible
- The effects of the thermal capacitance of each borehole (grout, U-tube pipe wall, and the working fluid flowing in it) are negligible, so the heat transfer inside the boreholes is effectively quasi-steady

- In the working fluid flowing in the U-tube pipe in each of the boreholes, conduction in the axial (or mean flow) direction (z) is negligible compared to advection, viscous dissipation is negligible, the thermophysical properties are constant (equal to values at the arithmetic-mean of the inlet and outlet bulk temperatures), and hydrodynamically and thermally fully developed turbulent flow prevails [Incropera and DeWitt (2002)]

The assumptions of effectively steady and two-dimensional groundwater flow in the horizontal cross-section of the borehole field, and negligible effects of buoyancy, can be avoided by using a numerical solution of the unsteady, three-dimensional, versions of the volume-averaged continuity and Darcy-Brinkman-Forchheimer equations (including buoyancy terms) [Vafai (2005); Nield and Bejan (2013)]. Furthermore, the assumption of quasi-steady heat transfer in the boreholes can be avoided by using a thermal-resistance-capacitance model (TRCM), similar to the one proposed by Bauer et al. (2011), and getting guidance from the works of Pasquier and Marcotte (2012) and Beier (2014). However, the above-mentioned assumptions were invoked in this work to keep the demonstration of the proposed hybrid method relatively simple and cost-effective, and the aforementioned ways to avoid these assumptions are considered as potential extensions of the work presented in this paper.

3.2. Groundwater flow

The following volume-averaged continuity and Darcy-Brinkman-Forchheimer equations [Vafai and Tien (1981); Vafai (2005); Nield and Bejan (2013)] were used to model the steady two-dimensional groundwater flow in the horizontal cross-section of the borehole field:

$$\frac{\partial}{\partial x} u_x + \frac{\partial}{\partial y} u_y = 0 \quad (1)$$

$$\begin{aligned}
\frac{\rho_w}{\varepsilon^2} \left(u_x \frac{\partial}{\partial x} u_x + u_y \frac{\partial}{\partial y} u_x \right) &= -\frac{\partial}{\partial x} P + \frac{\mu_w}{\varepsilon} \left(\frac{\partial^2}{\partial x^2} u_x + \frac{\partial^2}{\partial y^2} u_x \right) - \frac{\mu_w}{K} u_x - \frac{\rho_w C_F}{\sqrt{K}} u u_x \\
\frac{\rho_w}{\varepsilon^2} \left(u_x \frac{\partial}{\partial x} u_y + u_y \frac{\partial}{\partial y} u_y \right) &= -\frac{\partial}{\partial y} P + \frac{\mu_w}{\varepsilon} \left(\frac{\partial^2}{\partial x^2} u_y + \frac{\partial^2}{\partial y^2} u_y \right) - \frac{\mu_w}{K} u_y - \frac{\rho_w C_F}{\sqrt{K}} u u_y
\end{aligned} \tag{2}$$

In Eqs. (1) and (2), u_x and u_y are the groundwater Darcy (or superficial or phase-average) velocity components in the x and y directions, respectively; ρ_w and μ_w are the groundwater density and dynamic viscosity, respectively; ε and K are the porosity and permeability of the soil in the borehole field, respectively; C_F is the Forchheimer drag coefficient (it is assumed to be given by the Ergun equation, $C_F = \frac{1.75}{\sqrt{150\varepsilon^3}}$); $u = \sqrt{u_x^2 + u_y^2}$ is the magnitude of the groundwater Darcy velocity; and P is the intrinsic-phase-average reduced pressure (static pressure minus hydrostatic pressure) in the groundwater.

With reference to the geometry of the borehole field and the notation presented in Figs. 1 and 2, Dirichlet-type boundary conditions were prescribed for the Darcy velocity components at all domain boundaries; and these velocity components were set equal to zero at the interface between the ground and the outer wall of the boreholes ($\Gamma_{b,n}$ for borehole n), which was possible because of the inclusion of the Brinkman term in Eq. (2). These boundary and interface conditions can be expressed as follows:

$$u_x = U_\infty, u_y = 0, \text{ on } \Gamma_W, \Gamma_E, \Gamma_N, \Gamma_S \tag{3}$$

$$u_x = 0, u_y = 0, \text{ on all } \Gamma_{b,n} \tag{4}$$

It is useful at this stage to also examine the following dimensionless forms of the continuity and Darcy-Brinkman-Forchheimer equations:

$$\frac{\partial}{\partial x^*} u_x^* + \frac{\partial}{\partial y^*} u_y^* = 0 \tag{5}$$

$$\begin{aligned} \frac{1}{\varepsilon^2} \left(u_x^* \frac{\partial}{\partial x^*} u_x^* + u_y^* \frac{\partial}{\partial y^*} u_x^* \right) &= -\frac{\partial}{\partial x^*} P^* + \frac{1}{\varepsilon Re_{d_b}} \left(\frac{\partial^2}{\partial x^{*2}} u_x^* + \frac{\partial^2}{\partial y^{*2}} u_x^* \right) - \frac{1}{Re_{d_b} Da} u_x^* - \frac{C_F}{\sqrt{Da}} u_x^* u_x^* \\ \frac{1}{\varepsilon^2} \left(u_x^* \frac{\partial}{\partial x^*} u_y^* + u_y^* \frac{\partial}{\partial y^*} u_y^* \right) &= -\frac{\partial}{\partial y^*} P^* + \frac{1}{\varepsilon Re_{d_b}} \left(\frac{\partial^2}{\partial x^{*2}} u_y^* + \frac{\partial^2}{\partial y^{*2}} u_y^* \right) - \frac{1}{Re_{d_b} Da} u_y^* - \frac{C_F}{\sqrt{Da}} u_y^* u_y^* \end{aligned} \quad (6)$$

In Eqs. (5) and (6), $x^* = x/d_b$ and $y^* = y/d_b$ are dimensionless Cartesian coordinates, where $d_b = 2r_b$ is the diameter of the borehole; $u_x^* = u_x/U_\infty$ and $u_y^* = u_y/U_\infty$ are the dimensionless Darcy velocity components; $u^* = u/U_\infty$ is the magnitude of the dimensionless Darcy velocity; $P^* = P/(\rho_w U_\infty^2)$ is the dimensionless intrinsic-phase-average reduced pressure; $Re_{d_b} = \rho_w U_\infty d_b / \mu_w$ is the Reynolds number based on U_∞ and d_b ; and $Da = K/d_b^2$ is the Darcy number. The dimensionless boundary conditions are: $u_x^* = 1$, $u_y^* = 0$, on Γ_W , Γ_E , Γ_N , Γ_S ; and $u_x^* = 0$, $u_y^* = 0$, on all $\Gamma_{b,n}$. These boundary and interface conditions involve dimensionless geometric parameters that characterize the horizontal cross-section of the borehole field (Fig. 2).

3.3. Temperature distribution and heat transfer in the groundwater-saturated soil

In the context of the assumptions given in Section 3.1, the following volume-averaged unsteady three-dimensional advection-conduction equation [Vafai (2005); Nield and Bejan (2013)] was used to model the temperature of the groundwater-saturated soil in the borehole field:

$$(\rho c_p)_{eff} \frac{\partial T}{\partial t} + \rho_w c_{p,w} \left(u_x \frac{\partial T}{\partial x} + u_y \frac{\partial T}{\partial y} \right) = k_{eff} \left(\frac{\partial^2 T}{\partial x^2} + \frac{\partial^2 T}{\partial y^2} + \frac{\partial^2 T}{\partial z^2} \right) \quad (7)$$

In Eq. (7), $T = T(x, y, z, t)$ is the local volume-averaged ground temperature (the soil particles and the groundwater are assumed to be in local thermodynamic equilibrium); ρ_w and $c_{p,w}$ are the groundwater density and specific heat at constant pressure, respectively; $(\rho c_p)_{eff} = \varepsilon \rho_w c_{p,w} + (1 - \varepsilon) \rho_s c_{p,s}$ is the effective volumetric heat capacity of the groundwater-saturated soil, with ρ_s and $c_{p,s}$ denoting the density and specific heat at constant pressure of the dry soil, respectively; and k_{eff} is the effective thermal conductivity of the groundwater-saturated soil. In this work,

values of k_{eff} that are typical of groundwater-saturated soils commonly encountered in borehole fields were used (they are given later in this paper).

The following initial condition on the groundwater-saturated soil temperature was used: $T(x, y, z, 0) = T_g$. Here, T_g is the uniform undisturbed ground (and groundwater) temperature far from the boreholes. With reference to Fig. 2, Dirichlet-type boundary conditions for the groundwater-saturated soil temperature were imposed at the west, north, south, top, and bottom boundaries, denoted by Γ_W , Γ_N , Γ_S , Γ_T , and Γ_B , respectively. An outflow-type boundary condition [Patankar (1980)] was prescribed at the east boundary, denoted by Γ_E (in other words, advection heat transfer was considered to dominate conduction heat transfer at Γ_E). These boundary conditions can be expressed as follows:

$$T = T_g \text{ on } \Gamma_W, \Gamma_N, \Gamma_S, \Gamma_T, \Gamma_B \quad (8)$$

$$\frac{\partial}{\partial x} T = 0 \text{ on } \Gamma_E \quad (9)$$

In this mathematical model, the vertical boreholes were considered to extend to the ground surface ($z = 0$) and down to a length L_B below the active (or heated) length, H ; thus, their total length is equal to $(D + H + L_B)$. The interface between the ground and the outer wall of each of the boreholes (denoted by $\Gamma_{b,n}$ for borehole n) was considered adiabatic above and below their active length, $z < D$ and $z > (D + H)$, respectively. Over the active length, H , of each borehole, at the interface $\Gamma_{b,n}$, the rate of heat extraction was considered uniform over the borehole perimeter and variable along its length. For each borehole n , this interfacial condition over its active length can be expressed as follows:

$$(k_{eff} \nabla T \cdot \vec{n})_{b,n} = q''_{b,n}(z, t) \text{ on } \Gamma_{b,n} \text{ over } (D \leq z \leq D + H) \quad (10)$$

where \vec{n} is a unit normal pointing from the borehole outer wall into the ground; and $q''_{b,n}(z, t)$ is

the heat flux at $\Gamma_{b,n}$. It should be noted that $q''_{b,n}(z, t)$ varies with z and t , and it is considered positive when heat is extracted from the ground.

The above-mentioned mathematical model was solved numerically using a method that was formulated by amalgamating ideas adapted from a finite volume method (FVM) and a control-volume finite element method (CVFEM) described in the works of Baliga and Atabaki (2006) and Lamoureux and Baliga (2011). A brief overview of this CVFEM-FVM method is presented in Section 4. In this numerical solution, the groundwater Darcy velocity components u_x and u_y are specified using the corresponding CVFEM solution of the mathematical model presented in Section 3.2; and the values of heat flux $q''_{b,n}(z, t)$ are obtained using a quasi-steady, quasi-one-dimensional, semi-analytical model of the heat transfer in the boreholes, including the working fluid flowing through them (described in Subsection 3.4).

Eq. (7) was cast in the following dimensionless form in this work:

$$\frac{\Lambda}{Re_{d_b} Pr_w} \frac{\partial \theta}{\partial t^*} + \left(u_x^* \frac{\partial \theta}{\partial x^*} + u_y^* \frac{\partial \theta}{\partial y^*} \right) = \frac{\Upsilon}{Re_{d_b} Pr_w} \left(\frac{\partial^2 \theta}{\partial x^{*2}} + \frac{\partial^2 \theta}{\partial y^{*2}} + \frac{\partial^2 \theta}{\partial z^{*2}} \right) \quad (11)$$

In Eq. (11), $\theta = T_g - T / (\overline{|q''_b|} d_b / k_w)$ is the dimensionless temperature, with $\overline{|q''_b|} = |q_{total}| / (\pi d_b H N_b)$ denoting the absolute value of the heat flux at the interface between the boreholes and the groundwater-saturated soil, averaged over the outer surfaces of all N_b boreholes and over a suitable time period; $t^* = k_w t / (\rho_w c_{p,w} d_b^2)$ is the dimensionless time; the groundwater Prandtl number is $Pr_w = \mu_w c_{p,w} / k_w$; $\Lambda = (\rho c_p)_{eff} / (\rho_w c_{p,w}) = \{\varepsilon + (1 - \varepsilon) \rho_s c_{p,s} / (\rho_w c_{p,w})\}$; and $\Upsilon = k_{eff} / k_w$. The dimensionless initial condition is given by $\theta = 0$ at $t^* = 0$. The dimensionless boundary conditions are the following: $\theta = 0$ on $\Gamma_W, \Gamma_N, \Gamma_S, \Gamma_T, \Gamma_B$; and $\partial \theta / \partial x^* = 0$ on Γ_E . The dimensionless form of Eq. (10) is $(\Upsilon \nabla^* \theta \cdot \vec{n})_{b,n} = [q''_{b,n}(z, t) / \overline{|q''_b|}]$ on the interface $\Gamma_{b,n}$ over the dimensionless active length of

the borehole $\{(D/d_b) \leq z^* \leq (D + H)/d_b\}$. These boundary and interface conditions lead to dimensionless geometric parameters that characterize the borehole field (Figs. 1 and 2).

3.4. Working-fluid bulk temperature distribution and heat transfer in each borehole

Invoking the assumptions listed in Subsection 3.1, the heat transfer in the horizontal cross-section of the active portion ($D \leq z \leq D + H$) of each borehole, say n as illustrated in Figs. 1 and 3, can be modelled using a delta circuit of thermal resistances between the bulk temperatures of the working fluid circulating in the two legs (labelled as 1 and 2) of the U-tube pipe, $T_{f,1,n}(z)$ and $T_{f,2,n}(z)$, and the perimeter-average temperature of the borehole outer surface, $\bar{T}_{b,n}(z)$, as shown in Fig. 3.

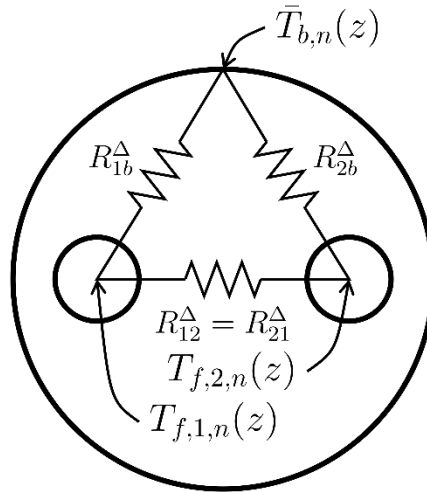


Figure 3. Horizontal cross-section of the active portion of borehole n , and the corresponding notation, thermal resistances (for unit length of the borehole), and delta circuit

For the vertical borehole with a single U-tube pipe symmetrically inserted in it and positioned in place with grout (see Figs. 1 and 3), a line-source approximation proposed by Hellström (1991) was used to obtain the following expressions for the thermal resistances (for unit length of the borehole) in the delta circuit illustrated in Fig. 3:

$$R_{1b}^{\Delta} = R_{2b}^{\Delta} = R_{11}^o + R_{22}^o ; R_{12}^{\Delta} = R_{21}^{\Delta} = \frac{R_{11}^o R_{22}^o + (R_{12}^o)^2}{R_{12}^o} \quad (12)$$

$$R_{11}^o = R_{22}^o = \frac{1}{2\pi k_g} \left[\ln \left(\frac{d_b}{d_{p,o}} \right) - \left(\frac{k_g - k_{eff}}{k_g + k_{eff}} \right) \ln \left(\frac{d_b^2}{d_b^2 - d_{1-2}^2} \right) \right] + R_p \quad (13)$$

$$R_{12}^o = \frac{1}{2\pi k_g} \left[\ln \left(\frac{d_b}{d_{1-2}} \right) + \left(\frac{k_g - k_{eff}}{k_g + k_{eff}} \right) \ln \left(\frac{d_b^2}{d_b^2 + d_{1-2}^2} \right) \right] \quad (14)$$

In Eqs. (13) and (14), k_g denotes the thermal conductivity of the grout that is used to hold the U-tube pipe within each borehole; $d_b = 2r_b$ is the diameter of the borehole; $d_{p,o} = 2r_{p,o}$ is the outer diameter of each leg of the U-tube pipe; k_{eff} is the effective thermal conductivity of the groundwater-saturated soil outside the borehole; d_{1-2} is the total distance between the centers of the cross-sections of the two legs, 1 and 2, of the U-tube pipe; and R_p is the thermal resistance (for unit length of the borehole) between the working fluid and the outer surface of the U-tube pipe wall. Higher-order procedures to obtain thermal resistances for symmetrically and non-symmetrically placed single and multiple U-tube pipes within each borehole are available in the works of Hellström (1991), Claesson and Hellström (2011), and Javed and Spitler (2017), for example.

The thermal resistance R_p in Eq. (13) is the sum of the forced-convection and pipe-wall thermal resistances (for unit length of the borehole):

$$R_p = \frac{1}{\pi d_{p,i} h_f} + \frac{\ln(d_{p,o}/d_{p,i})}{2\pi k_p} \quad (15)$$

In Eq. (15), k_p denotes the thermal conductivity of the pipe-wall material; $d_{p,i} = 2r_{p,i}$ is the inner diameter of each leg of the U-tube pipe; and h_f is the forced-convection heat transfer

coefficient on the inner surface of each leg of the U-tube pipe. In this work, h_f was obtained using the Gnielinski correlation [Incropera and DeWitt (2002)]:

$$\frac{h_f d_{p,i}}{k_f} = \frac{(f/8)(Re_{f,d_{p,i}} - 1000)Pr_f}{1 + 12.7(f/8)^{0.5}(Pr_f^{2/3} - 1)} \quad (16)$$

In Eq. (16), k_f is the thermal conductivity of the working fluid flowing in the U-tube pipe; $Re_{f,d_{p,i}} = \frac{4\dot{m}_f}{\pi\mu_f d_{p,i}}$ is the Reynolds number of the working fluid, with \dot{m}_f and μ_f denoting its mass flow rate (in each U-tube pipe) and dynamic viscosity, respectively; $Pr_f = \mu_f c_{p,f}/k_f$ is the Prandtl number of the working fluid, with $c_{p,f}$ denoting its specific heat at constant pressure; and f is the Darcy friction factor. In this work, the Colebrook correlation [Incropera and DeWitt (2002)] was used to obtain f :

$$\frac{1}{\sqrt{f}} = -2 \log_{10} \left(\frac{e_{rms}/d_{p,i}}{3.7} + \frac{2.51}{Re_{f,d_{p,i}} \sqrt{f}} \right) \quad (17)$$

where e_{rms} is the root-mean-square roughness of the inner surface of the pipe wall.

With the assumptions listed in Subsection 3.1, $T_{f,1,n}(z)$ and $T_{f,2,n}(z)$ are governed by the following equations (note that the coordinate $z = 0$ at the ground surface of the borehole field and increases vertically downwards, as shown in Fig. 1; and the working fluid flows in legs 1 and 2 of the U-tube pipe in the positive and negative z directions, respectively):

$$(\dot{m}_f c_{p,f}) \frac{\partial T_{f,1,n}(z)}{\partial z} = \frac{(\bar{T}_{b,n}(z) - T_{f,1,n}(z))}{R_{1b}^\Delta} + \frac{(T_{f,2,n}(z) - T_{f,1,n}(z))}{R_{12}^\Delta} \quad (18)$$

$$-(\dot{m}_f c_{p,f}) \frac{\partial T_{f,2,n}(z)}{\partial z} = \frac{(\bar{T}_{b,n}(z) - T_{f,2,n}(z))}{R_{2b}^\Delta} + \frac{(T_{f,1,n}(z) - T_{f,2,n}(z))}{R_{21}^\Delta} \quad (19)$$

In the proposed model, the working-fluid mass flow rate in each borehole, \dot{m}_f , is specified; the perimeter-average temperature of the outer surface of the borehole, $\bar{T}_{b,n}(z)$, is prescribed (calculated at any time, t , from a numerical solution to the model of the unsteady three-dimensional temperature and heat transfer in the groundwater-saturated soil of the borehole field); and the total rate of heat extraction from the ground, q_{total} , from all N_b boreholes in the field of interest is specified as a function of time, t . The working fluid enters the active portion of borehole n at a bulk temperature $T_{f,in,n}$ in leg 1 of the U-tube pipe, and it leaves the active portion of this borehole through leg 2 of this pipe at a bulk temperature $T_{f,out,n}$. At any time, t , the values of $T_{f,in,n}$ for all N_b boreholes are assumed to be the same, $T_{f,in}$; and this value is adjusted to achieve the specified value of q_{total} .

The following set of dimensionless parameters characterize the above-mentioned mathematical model: $Re_{f,d_{p,i}} = \frac{4\dot{m}_f}{\pi\mu_f d_{p,i}}$; $Pr_f = \mu_f c_{p,f}/k_f$; $(e_{rms}/d_{p,i})$; (k_p/k_w) ; $(d_{p,o}/d_b)$; $(d_{p,i}/d_b)$; and (d_{1-2}/d_b) .

An extension of this model to boreholes with multiple U-tube pipes can be achieved using the ideas presented in the works of Zeng et al. (2003), Eslami-Nejad and Bernier (2011), Belzile et al. (2016), and Cimmino (2016). A semi-analytical method was used to solve the above-mentioned quasi-steady, quasi-one-dimensional, mathematical model of the working-fluid bulk-temperature distribution and heat transfer in the boreholes. This semi-analytical method is concisely described in Subsection 4.3.

4. Numerical and semi-analytical methods

The numerical and semi-analytical methods that were used to solve the mathematical models presented in Section 3 are described concisely in this section.

4.1. Overview of the numerical method used for solving the mathematical model of the groundwater flow in the borehole field

A co-located equal-order CVFEM [Baliga and Atabaki (2006); Lamoureux and Baliga (2011); Baliga et al. (2017)] was used to solve the mathematical model of the steady two-dimensional groundwater flow presented in Subsection 3.2. This CVFEM was implemented to work with unstructured planar grids of three-node triangular elements and polygonal control volumes associated with the vertices of the elements. A mesh generator written in Matlab by Persson and Strang (2004) was used in this work to create the unstructured planar grid of three-node triangular elements. A sample unstructured grid of three-node triangular elements used for discretizing a horizontal cross-section of a 3 x 2 borehole field is shown in Fig. 4 (top), along with the details of this grid in the vicinity of the six boreholes (center) and one borehole (bottom). Additional details of the grids that were used for obtaining the results presented in this paper are given in Section 5.

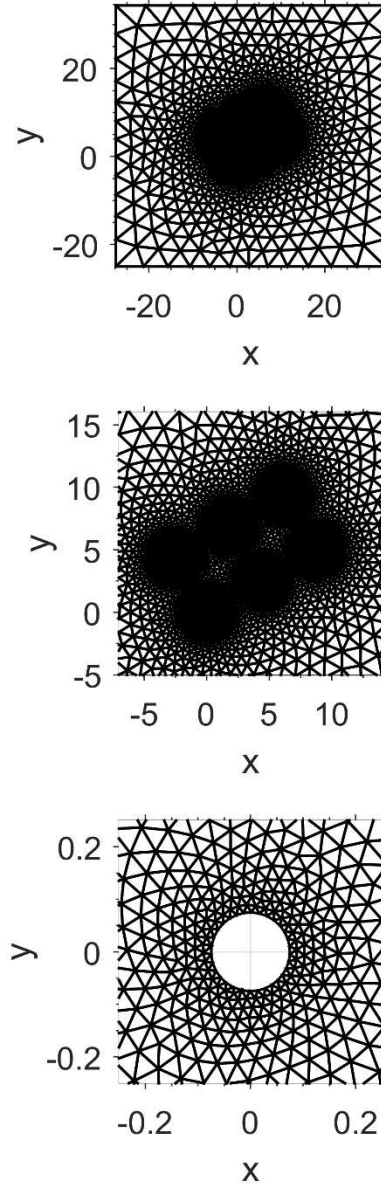


Figure 4. Discretization of a horizontal cross-section of a 3 x 2 borehole field using an unstructured grid of three-node triangular elements (top), and the details of this grid in the vicinity of the six boreholes (center) and one borehole (bottom)

Each triangular element in the unstructured grid (Fig. 4) used in the above-mentioned CVFEM is divided into three equal areas by joining its centroid to the mid-points of its three sides; and these equal areas in each triangular element collectively create polygonal control volumes (of unit depth) around each vertex in the finite-element grid. The governing equations

are integrated over the polygonal control volumes to obtain integral conservation equations. The dependent variables and the effective thermophysical properties involved in the governing equations are interpolated in each triangular element as follows: P is interpolated linearly; u_x and u_y are interpolated using a linear function in the viscous transport terms and a flow-oriented (FLO) scheme in the advection terms [Baliga and Aatabaki (2006)]; in the Darcy and Forchheimer terms, the nodal values of u_x and u_y are assumed to prevail over the three corresponding portions of the control volumes within the triangular element; and the centroidal values of ρ_w , μ_w , ε , K , and C_F are assumed to prevail over the triangular element. In the velocity components that appear in the mass-fluxes ($\rho_w u_x$ and $\rho_w u_y$) in the advection terms of the Darcy-Brinkman-Forchheimer equations, the groundwater Darcy velocity components are interpolated using the so-called momentum-interpolation scheme to avoid checkerboard-type pressure distributions in the co-located equal-order formulation of the CVFEM [Rhie and Chow (1983); Baliga and Aatabaki (2006)]. These interpolation functions are used to obtain the discretized equations, which are algebraic approximations to the integral conservation equations. The above-mentioned CVFEM is second-order-accurate.

A sequential iterative variable adjustment (SIVA) procedure was used to solve the non-linear and coupled sets of discretized (algebraic) equations. In every overall iteration of this SIVA procedure, linearized and decoupled sets of discretized equations for the dependent variables were solved sequentially using a bi-conjugate gradient method [Saad (2003)]. For each set of input parameters in the problems of interest, the CVFEM solution for the steady, two-dimensional, groundwater flow was obtained only once, and the corresponding time-invariant values of the Darcy velocity components were stored and used over the full time period of operation of the borehole field. An extension of this model to layered ground with varying

hydraulic properties and groundwater flow velocities could be achieved by solving the mathematical model of the steady two-dimensional groundwater flow for each subsurface layer separately. The resulting groundwater velocities could then be applied to the corresponding nodes of the three-dimensional grid for solving the complementary heat transfer problem.

4.2. Overview of the numerical method used for solving the mathematical model of the temperature and heat transfer in the groundwater-saturated soil of the borehole field

The proposed mathematical model of the unsteady three-dimensional temperature distribution in the groundwater-saturated soil of the borehole field was solved numerically using a CVFEM-FVM that was formulated by amalgamating ideas described in the works of Baliga and Atabaki (2006) and Lamoureux and Baliga (2011). This method was implemented to work with a three-dimensional grid that is obtained by traversing the unstructured two-dimensional grid of triangular elements (in the horizontal cross-section of the borehole field; see Fig. 4) in the vertical (z) direction, to generate prismatic pentahedral elements and control volumes of triangular and polygonal cross-sections, respectively, in the horizontal plane. A vertical cross-section of such a grid in the region adjacent to the boundary $\Gamma_{b,n}$ of a borehole n is illustrated in Fig. 5: the total number of nodes (grid points) in the vertical (z) direction is denoted by N_z ; the vertical extent of the control volume associated with the node k is denoted by Δz_k , for $k = \{1, 2, \dots, N_z\}$; the control volume associated with the nodes along the top (Γ_T) and bottom (Γ_B) boundaries have zero-thickness in the z direction ($\Delta z_1 = \Delta z_{N_z} = 0$); and the internal nodes $k = \{2, 3, \dots, N_z - 1\}$ are located in the z direction at the geometric centers of the Δz_k extents of their respective control volumes. The proposed numerical method was formulated to work with a non-uniform distribution of Δz_k .

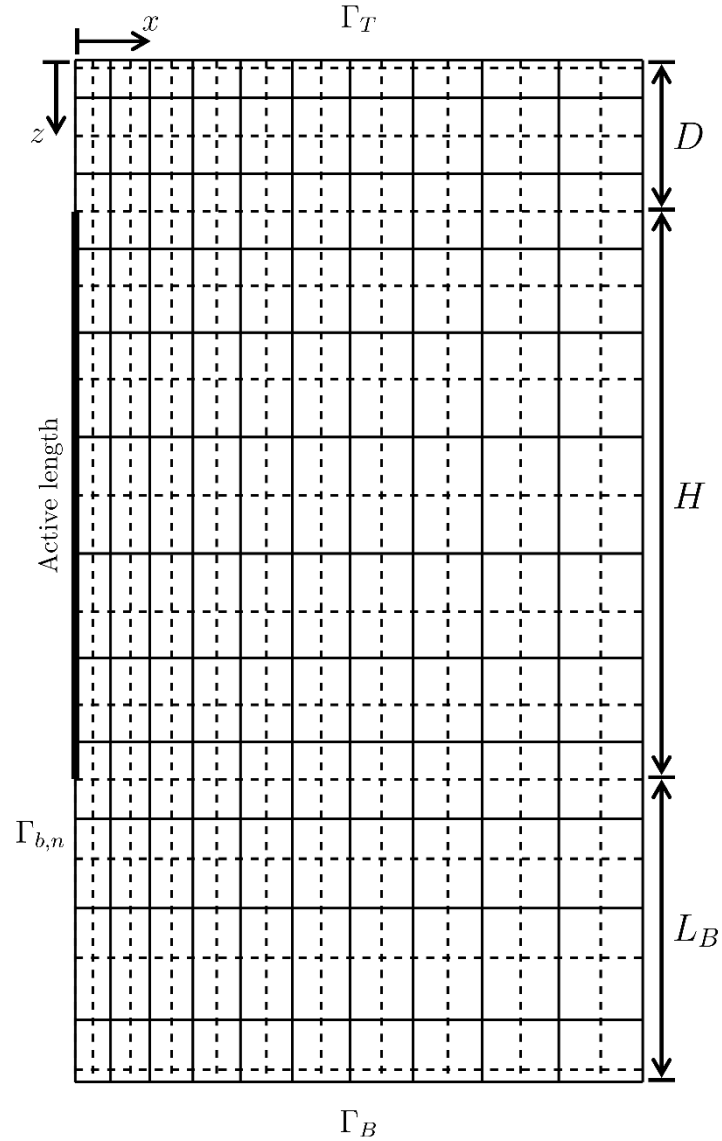


Figure 5. A vertical (x - z) cross-section of a representative three-dimensional grid of pentahedral elements in a region adjacent to the boundary $\Gamma_{b,n}$ of borehole n (the intersections of the solid lines denote grid points; and the control-volume faces are indicated by dashed lines).

In the CVFEM-FVM that was formulated and used for solving the unsteady three-dimensional temperature distribution in the groundwater-saturated soil of the borehole field, the dependent variables and the effective thermophysical properties involved in the governing equations are spatially interpolated in each pentahedral element as follows: 1) in the horizontal (x,y) planes of the grid, which consist of the unstructured mesh of three-node triangular

elements, the interpolation functions are the same as those mentioned above for the two-dimensional CVFEM; 2) in the vertical (z) direction, the centroidal values of the effective thermophysical properties are interpolated using a resistance analogy scheme (which reduces to the harmonic mean if uniform grids are used), the hybrid scheme is used to interpolate T in the advection and conduction transport terms, the momentum interpolation scheme is used to interpolate the velocity components in the mass flux terms, and quadratic functions are used to interpolate T in the conduction terms adjacent to the top and bottom boundaries (where $\Delta z_1 = \Delta z_{N_z} = 0$) [Patankar (1980); Rhie and Chow (1983); Baliga and Atabaki (2006)]. These discretizations of the spatial terms in the three-dimensional CVFEM-FVM are second-order-accurate.

In the proposed CVFEM-FVM, for each time step, Δt , the above-mentioned spatial interpolation functions and the fully-implicit time-integration scheme [Patankar (1980)] (based on a backward Euler method) are used to obtain the discretized equations, which are algebraic approximations to the integral conservation equations applied to the above-mentioned prismatic control volumes. These discretized equations, which are non-linear, in general, are solved iteratively in each time step: the coefficients in a set of linearized discretized equations are calculated using the latest available values of T ; the linearized set of discretized equations is solved using a bi-conjugate gradient method [Saad (2003)]; and these steps are repeated until convergence. The aforementioned time-integration scheme is first-order-accurate.

4.3. Semi-analytical method used for solving the mathematical model of the working-fluid bulk-temperature distribution and heat transfer in each borehole

A semi-analytical method was used to solve the quasi-steady, quasi-one-dimensional, mathematical model of the working-fluid bulk-temperature distribution and heat transfer in each

borehole. In this semi-analytical method, the vertical boreholes are discretized into N_z segments in the vertical (z) direction; Δz_k denotes the vertical extent of the segment k in the z direction; $z_{face,k}$ denotes the bottom face of the segment k in the z direction (which points downwards); and $z_{face,k-1}$, $z_{face,k}$, and Δz_k match up perfectly with the corresponding z -coordinates of the faces and extents of the prismatic control volumes in the CVFEM-FVM numerical method described in the previous section. The active portion of each vertical borehole ($D \leq z \leq D + H$) is discretized into $N_{z,ac}$ nodes and segments in the vertical direction; and $k_{1,ac}$ and $k_{N_{z,ac}}$ are used to denote the first and last nodes in this active portion of the borehole. The general solutions to Eqs. (18) and (19) for an arbitrary $\bar{T}_{b,k,n}(z)$ profile along the active length of the borehole are given below [Eskilson and Claesson (1988); Hellström (1991)]:

$$T_{f,1,n}(z') = T_{f,in,n}f_1(z') + T_{f,out,n}f_2(z') + \int_0^{z'} \bar{T}_{b,n}(z'')f_4(z' - z'')dz'' \quad (20)$$

$$T_{f,2,n}(z') = -T_{f,in,n}f_2(z') + T_{f,out,n}f_3(z') - \int_0^{z'} \bar{T}_{b,n}(z'')f_5(z' - z'')dz'' \quad (21)$$

$$T_{f,out,n} = \frac{f_1(H)+f_2(H)}{f_3(H)-f_2(H)}T_{f,in,n} + \int_0^H \frac{\bar{T}_{b,n}(z'')[f_4(H-z'')+f_5(H-z'')]}{f_3(H)-f_2(H)} dz'' \quad (22)$$

with $z' = z - D$, and

$$f_1(z') = \exp(\beta z') [\cosh(\gamma z') - \delta \sinh(\gamma z')] \quad (23)$$

$$f_2(z') = \exp(\beta z') \frac{\beta_{12}}{\gamma} \sinh(\gamma z') \quad (24)$$

$$f_3(z') = \exp(\beta z') [\cosh(\gamma z') + \delta \sinh(\gamma z')] \quad (25)$$

$$f_4(z') = \exp(\beta z') \left[\beta_1 \cosh(\gamma z') - \left(\delta \beta_1 + \frac{\beta_2 \beta_{12}}{\gamma} \right) \sinh(\gamma z') \right] \quad (26)$$

$$f_5(z') = \exp(\beta z') \left[\beta_2 \cosh(\gamma z') + \left(\delta \beta_2 + \frac{\beta_1 \beta_{12}}{\gamma} \right) \sinh(\gamma z') \right] \quad (27)$$

$$\beta_1 = \frac{1}{R_{1b}^\Delta \dot{m}_f c_{p,f}}; \quad \beta_2 = \frac{1}{R_{2b}^\Delta \dot{m}_f c_{p,f}}; \quad \beta_{12} = \frac{1}{R_{12}^\Delta \dot{m}_f c_{p,f}}; \quad \beta = \frac{\beta_2 - \beta_1}{2} \quad (28)$$

$$\gamma = \sqrt{\frac{(\beta_1 + \beta_2)^2}{4} + \beta_{12}(\beta_1 + \beta_2)}; \quad \delta = \frac{1}{\gamma} \left(\beta_{12} + \frac{\beta_1 + \beta_2}{2} \right) \quad (29)$$

In the proposed semi-analytical method, the perimeter-average temperature of the outer surface of the segment k of a borehole n , $\bar{T}_{b,k,n}$, is assumed to be piecewise uniform over the perimeter (πd_b) and the length ($z_{face,k} - z_{face,k-1}$) of the segment. With this assumption and the above-mentioned discretization of the length of each borehole (and with $z'_k = z_k - D$), the integrals in Eqs. (20) to (22) can be solved analytically in the active portions of the boreholes and these equations can be cast as follows:

$$T_{f,1,n}(z'_{face,k_{i,ac}}) = T_{f,in,n} f_1(z'_{face,k_{i,ac}}) + T_{f,out,n} f_2(z'_{face,k_{i,ac}}) + \sum_{j=k_{1,ac}}^{k_{i,ac}} \bar{T}_{b,j,n} \left[F_4(z'_{face,k_{i,ac}} - z'_{face,k_{j-1}}) - F_4(z'_{face,k_{i,ac}} - z'_{face,k_j}) \right] \quad (30)$$

$$T_{f,2,n}(z'_{face,k_{i,ac}}) = -T_{f,in,n} f_2(z'_{face,k_{i,ac}}) + T_{f,out,n} f_3(z'_{face,k_{i,ac}}) - \sum_{j=k_{1,ac}}^{k_{i,ac}} \bar{T}_{b,j,n} \left[F_5(z'_{face,k_{i,ac}} - z'_{face,k_{j-1}}) - F_5(z'_{face,k_{i,ac}} - z'_{face,k_j}) \right] \quad (31)$$

$$T_{f,out,n} = \frac{f_1(H) + f_2(H)}{f_3(H) - f_2(H)} T_{f,in,n} +$$

$$\sum_{j=k_{1,ac}}^{k_{N_z,ac}} \frac{\bar{T}_{b,k_j,n}}{f_3(H)-f_2(H)} \left[F_4 \left(H - z'_{f_{ace},k_{j-1}} \right) - F_4 \left(H - z'_{f_{ace},k_j} \right) + F_5 \left(H - z'_{f_{ace},k_{j-1}} \right) - F_5 \left(H - z'_{f_{ace},k_j} \right) \right] \quad (32)$$

with

$$F_4(z') = \int_0^{z'} f_4(z' - z'') dz'' = \exp(\beta z') \left[-\cosh(\gamma z') + \frac{\beta_1 + \beta_2}{2\gamma} \sinh(\gamma z') + 1 \right] \quad (33)$$

$$F_5(z') = \int_0^{z'} f_5(z' - z'') dz'' = \exp(\beta z') \left[\cosh(\gamma z') + \frac{\beta_1 + \beta_2}{2\gamma} \sinh(\gamma z') - 1 \right] \quad (34)$$

From an energy balance on the working fluid in both legs of the boreholes, using Eqs. (30) and (31), the values of the heat flux $q''_{b,k,n}(z, t)$ at the interfaces ($\Gamma_{b,n}$) between the active portion of the borehole n and the groundwater-saturated soil can be calculated using the following equation for the nodes $k = k_{1,ac}, \dots, k_{N_z,ac}$ (for the other nodes, the heat flux is zero):

$$q''_{b,k_{i,ac},n} = \frac{\dot{m}_f c_{p,f}}{\pi d_b \Delta z_{k_{i,ac}}} \left(\begin{array}{l} T_{f,1,n} \left(z'_{f_{ace},k_{i,ac}} \right) - T_{f,1,n} \left(z'_{f_{ace},k_{i,ac}-1} \right) + \\ T_{f,2,n} \left(z'_{f_{ace},k_{i,ac}-1} \right) - T_{f,2,n} \left(z'_{f_{ace},k_{i,ac}} \right) \end{array} \right) \quad (35)$$

In the same manner, using Eq. (32), the total heat extraction rate of the borehole n ($q_{b,n}$) and the total heat extraction rate over all N_b boreholes in the field (q_{total}) can be calculated from the following equations:

$$q_{b,n} = \dot{m}_f c_{p,f} \left(\left(\frac{f_1(H) + f_2(H)}{f_3(H) - f_2(H)} - 1 \right) T_{f,in,n} + \sum_{j=k_{1,ac}}^{k_{N_z,ac}} \frac{\bar{T}_{b,k_j,n}}{f_3(H) - f_2(H)} \left[F_4 \left(H - z'_{f_{ace},k_{j-1}} \right) - F_4 \left(H - z'_{f_{ace},k_j} \right) + F_5 \left(H - z'_{f_{ace},k_{j-1}} \right) - F_5 \left(H - z'_{f_{ace},k_j} \right) \right] \right) \quad (36)$$

$$q_{total} = \dot{m}_f c_{p,f} \left(N_b \left(\frac{f_1(H) + f_2(H)}{f_3(H) - f_2(H)} - 1 \right) T_{f,in} + \sum_{n=1}^{N_b} \sum_{j=k_{1,ac}}^{k_{N_z,ac}} \frac{\bar{T}_{b,k_j,n}}{f_3(H) - f_2(H)} \left[F_4 \left(H - z'_{face,k_{j-1}} \right) - F_4 \left(H - z'_{face,k_j} \right) + F_5 \left(H - z'_{face,k_{j-1}} \right) - F_5 \left(H - z'_{face,k_j} \right) \right] \right) \quad (37)$$

The values of the heat flux $q''_{b,k,n}(z, t)$ vary with z and t ; and when they are positive, heat is extracted from the ground. The calculated values of $q''_{b,k,n}(z, t)$ are provided as inputs to the numerical solution of the temperature distribution and heat transfer in the groundwater-saturated soil (using the CVFEM-FVM described in Subsection 4.2).

4.4. Summary of the overall numerical procedure

At each time, t , based on the known (specified) total rate of heat extraction, $q_{total}(t + \Delta t)$, the following overall iterative procedure is used to advance the solution from t to $t + \Delta t$.

1. Using Eq. (37), calculate the entering fluid temperature ($T_{f,in}$) that is required to satisfy the total rate of heat extraction with the latest values of perimeter-average outer-surface temperature of all borehole segments ($\bar{T}_{b,k,n}$).
2. Calculate the heat fluxes at the outer surface of all borehole active-portion segments ($q''_{b,k_i,ac,n}$), using Eqs. (30), (31), (32) and (35). Note that outside the active portions, the outer surface of the boreholes is assumed to be adiabatic, so the corresponding heat fluxes are zero.
3. With the latest values of the heat fluxes at the outer surface of all borehole segments (calculated in Step 2) as inputs to the numerical method described in Section 4.2, solve the mathematical model of the temperature and heat transfer in the groundwater-saturated soil of the borehole field, and then calculate the values of the perimeter-average outer-surface temperature of all borehole segments ($\bar{T}_{b,k,n}$).

4. Repeat steps 1-3 until convergence. In this work, convergence was assumed when the maximum absolute difference between two successive evaluations of the perimeter-average outer-surface temperature of all borehole segments ($\bar{T}_{b,k,n}$) was less than 0.01 °C.

5. Results

The results obtained for the following test and demonstration problems are presented and discussed in this section: 1) grid-independence checks on the results generated by the CVFEM-FVM described in Section 4, by applying it to a single-borehole field, with a prescribed uniform and constant heat flux on the outer-surface of the borehole; 2) comparisons of the CVFEM-FVM predictions for a 3 x 2 borehole field, with a prescribed uniform and constant heat flux on the outer-surface of each of the boreholes, and the results obtained using a moving-finite-line-source analytical solution to a simplified version of this problem; and 3) a two-year simulation of a 3 x 2 borehole field coupled to a ground-source heat-pump system. In these test and demonstration problems, the ranges of the required thermophysical properties for dry granular soils likely to be encountered in borehole fields were obtained from the published literature, such as the works of Chiasson et al. (2000) and Molina-Giraldo et al. (2011b), for example. The thermophysical properties of groundwater were taken to be the following [Incropera and DeWitt (2002)]: $\rho_w = 1000 \text{ kg/m}^3$; $c_{p,w} = 4190 \text{ J/kg-K}$; $k_w = 0.59 \text{ W/m-K}$; and $\mu_w = 0.00179 \text{ Pa-s}$ (at 0 °C) to 0.000798 Pa-s (at 30°C). A hydraulic gradient of 10^{-3} m/m and a borehole diameter $d_b = 0.15 \text{ m}$ were assumed. With these data, the ranges of soil Darcy number ($Da = K/d_b^2$), effective Péclet number ($Pe_{d_b} = Re_{d_b} Pr_w / \gamma = d_b U_\infty \rho_w c_{p,w} / k_{eff}$), effective volumetric thermal capacity ratio ($\Lambda = \frac{(\rho c_p)_{eff}}{\rho_w c_{p,w}}$), thermal conductivity ratio ($\gamma = \frac{k_{eff}}{k_w}$), and soil porosity (ε) were determined; and they are presented in Table 1.

Table 1. Ranges of some dimensionless parameters considered in this work.

Soil Type	Da		Pe_{d_b}		Y		A		Porosity (ϵ)	
	Min	Max	Min	Max	Min	Max	Min	Max	Min	Max
Gravel	3.62E-10	8.10E-08	3.49E-02	3.49E+00	3.05	3.05	0.573	0.573	0.24	0.38
Coarse Sand	3.62E-09	8.10E-09	1.26E-01	3.70E-01	2.88	8.47	0.525	0.692	0.31	0.46
Medium Sand	3.62E-10	8.10E-10	1.26E-02	3.70E-02	2.88	8.47	0.525	0.692	-	-
Fine Sand	3.62E-12	8.10E-11	1.26E-04	3.70E-03	2.88	8.47	0.525	0.692	0.26	0.53
Silt	3.62E-13	8.10E-13	2.73E-05	6.98E-05	1.53	3.90	0.382	0.811	0.34	0.61
Clay	3.62E-16	8.10E-15	4.19E-08	5.24E-07	2.03	2.54	0.549	0.549	0.34	0.60

From the results of initial exploratory numerical simulations, it was found that the effects of the Darcy number, Da , in the range of values given in Table 1, on the predicted temperatures in the problems of interest were negligible. This finding is in agreement with that of Thevenin and Sadaoui (1995), in which no influence of the Darcy number was observed for $Da < 10^{-6}$.

5.1. Grid-independence of the numerical predictions of temperature in the groundwater-saturated soil of a single-borehole field

The investigation reported in this subsection was undertaken to provide guidance in the choice of suitable grids for all of the test and demonstration problems considered in this work. In the grid-independence checks presented here, the case of a single borehole with a constant and uniform rate of heat extraction from the ground over its active portion ($D \leq z \leq D + H$) is considered. Attention could thus be focused solely on the temperature and heat transfer in the groundwater-saturated soil of the borehole field, without dealing with the heat transfer and temperature inside the boreholes and the working fluid flowing through the U-tube pipe within them. With reference to the notation given in Figs. 1 and 2, the borehole has a length $H = 150$ m, a diameter $d_b = 0.15$ m, and a buried depth $D = 4$ m. The borehole is centrally located within the horizontal

cross-section of the calculation domain, which has extents $L_W = L_E = L_N = L_S = 15$ m; and in the vertical direction, the calculation domain extends to $L_B = 50$ m below the active portion of the borehole. The full extents of the calculation domain, as shown in Figs. 1 and 2, are $L_X = L_Y = 30$ m and $L_Z = 204$ m. The values of the dimensionless parameters considered in the problem are the following: $Pe_{d_b} = 1$, $Da = 10^{-9}$, $Y = 3$, $\Lambda = 0.71$, and $\varepsilon = 0.34$; and on the outer surface of the single borehole, $(Y\nabla^*\theta \cdot \vec{n})_b = [q_b''(z, t)/|\overline{q_b''}|] = 1$ for $\{(D/d_b) \leq z^* \leq (D + H)/d_b\}$.

The baseline grid (denoted by $N = 1$) consists of 73,680 pentahedral elements and is generated from a two-dimensional grid of 2,456 triangular elements (constructed using the grid generator of Persson and Strang (2004)). The minimum side length of the triangular elements is $h_{min} = 0.0147$ m ($= \pi d_b / 32$) at the outer surface of the borehole. The side length of the triangular elements increases linearly at a rate of 0.167 m/m based on the distance to the closest borehole. The vertical discretization consists of $N_z = 32$ horizontal layers (including the top and bottom layers with zero thickness): two equal vertical layers of thickness 2 m are located above the active portion of the borehole; 20 vertical layers with a minimum thickness 2.25 m and a maximum thickness 16.80 m are located along the active portion of the borehole; and eight vertical layers with a minimum thickness of 2.52 m and a maximum thickness of 12.02 m are located below the active portion of the borehole. The thickness of successive vertical layers increase by a factor of about 1.25 from the top-most and the bottom-most layers along the active portion towards the center of the borehole, and from the top-most layer below the active portion towards the bottom of the three-dimensional grid. The time step corresponding to the baseline grid is $\Delta t = 600$ s.

A pattern-preserving grid-refinement technique and the extended Richardson extrapolation procedure proposed by Baliga and Lokhmanets (2016) were used in these grid-independence checks. The finer pattern-preserving spatial grids and time steps were obtained by subdividing the baseline spatial grid and time ($N = 1$) step by factors of two and four: to achieve the first and second refinements ($N = 2$ and 3), each triangular element of the two-dimensional grid in the horizontal cross-section was divided into 4 and 16 similar-shaped triangular elements of equal area, respectively; each vertical layer was divided into 2 and 4 layers of equal thickness, respectively; and the corresponding time step was divided by factors of 4 and 16, respectively.

Representative results of these grid-independence checks are summarized in Table 2. For $t = 1$ hour ($t^* = \frac{k_w t}{\rho_w c_p w d_b^2} = 0.023$), the values of the perimeter-average outer-surface dimensionless temperature of the borehole ($\bar{\theta}_b$) at the mid-point of its active portion (obtained with the aforementioned three grids, $N = 1, 2,$ and 3) and the extrapolated value obtained using the results of the second and third of these grids ($N = 2$ and 3) are presented: the absolute percentage difference between the value calculated from the baseline ($N = 1$) grid and the extrapolated value is 4.32 %, which is considered acceptable in this work, in the context of long-term (multi-annual) simulations of such geothermal systems. At $t = 4$ weeks ($t^* = 15.1$), the values of $\bar{\theta}_b$ at the mid-point of the active portion of the borehole, and also the dimensionless temperature (θ) at a distance of 5 m downstream from the borehole at the mid-point of its active portion ($x = 5$ m, $y = 0$, $z = D + H/2$; relative to the coordinate system presented in Figs. 1 and 2) are presented. These relatively long-term simulations ($t = 4$ weeks), were done with only two of the aforementioned grids ($N = 1$ and 2); the absolute percentage differences between the values obtained from baseline-grid and the corresponding extrapolated values are 0.11% for $\bar{\theta}_b$ and 5.23% for θ ; and these differences were also considered acceptable in this work.

Table 2. Representative results of the grid independence checks.

Number of elements	Temperature (Absolute % difference with the extrapolated value)		
	$t = 1 \text{ hour } (t^* = 0.023)$	$t = 4 \text{ weeks } (t^* = 15.1)$	$t = 4 \text{ weeks } (t^* = 15.1)$
	$\bar{\theta}_b(z = D + H/2)$	$\bar{\theta}_b(z = D + H/2)$	$\theta \left(\begin{matrix} x = 5\text{m}, y = 0\text{m}, \\ z = D + H/2 \end{matrix} \right)$
73,680 (=N)	0.08854 (4.32 %)	0.28525 (0.11 %)	0.04834 (5.23 %)
589,440 (=8N)	0.09154 (1.08 %)	0.28502 (0.03 %)	0.05034 (1.31 %)
4,715,520 (=64N)	0.09228 (0.27 %)	-	-
Extrapolated value	0.09253	0.28493	0.05101

Based on these grid-independence checks, the spatial grids and time steps used for the simulations reported in the next two sections were chosen to be similar to the above-mentioned baseline spatial grid and time step.

5.2. Comparison of the CVFEM-FVM predictions of the groundwater- saturated soil temperature with results obtained using a moving-finite-line-source method

In this problem, six boreholes (diameter $d_b = 0.15 \text{ m}$) arranged in a 3×2 array at an angle of $\beta_b = 30^\circ$ relative to the direction of groundwater flow (as shown on Figure 2) are considered, and the heat flux on the outer surface of the boreholes is specified to be uniform and constant. Attention in this problem can thus be focused solely on the temperature and heat transfer in the groundwater-saturated soil of the borehole field, without dealing with the heat transfer and temperature of the boreholes and the working fluid flowing through the U-tube pipe within them. The dimensionless parameters considered in this problem are following: $Da = 10^{-9}$, $\gamma = 3$, $\Lambda = 0.71$, $\varepsilon = 0.34$; two values of the Peclet number $Pe_{d_b} = 0.01$ and $Pe_{d_b} = 0.1$; and on the outer surface of the active portions of the boreholes, $(\gamma \nabla^* \theta \cdot \vec{n})_{b,n} = [q''_{b,n}(z, t) / \overline{|q''_b|}] = 1$ for $\{(D/d_b) \leq z^* \leq \{(D + H)/d_b\}$. The calculation domain extends to $L_W = L_E = L_N = L_S = 25 \text{ m}$ on all sides of the borehole array in the horizontal plane; and $H = 150 \text{ m}$ and $L_B = 50 \text{ m}$ (Fig. 1). The resulting total extents of the calculation domain are $L_X = 61.2 \text{ m}$,

$L_Y = 59.3$ m and $L_Z = 204$ m. The total time of the simulations in this problem is 2 years ($t^* = 395$). The groundwater flow is assumed to be governed by the mathematical model presented in Section 3.2, and predicted using the CVFEM described in Section 4.1. The temperature and heat transfer in the groundwater-saturated soil are assumed to be governed by the mathematical model presented in Section 3.3, except for the prescription of a uniform and constant heat flux on the outer surface of each of the six boreholes, and predicted using the unsteady three-dimensional CVFEM-FVM described in Section 4.2. The spatial grid and time step used in the numerical solution of this problem were chosen using guidance from the baseline grid and time step discussed in the grid-independence study described in Section 5.1. The resulting grid consists of 354,660 pentahedral elements and is generated from a two-dimensional grid of 11,822 triangular elements.

A simplified version of this problem was also solved analytically using a moving-finite-line-source technique, which applies strictly only to the ground temperature around a line source, moving at a constant velocity and emitting heat uniformly along its length at a constant rate. Thus, the geometry considered in this moving-finite-line-source solution differs from the one considered in the numerical model, where heat is emitted from the impermeable cylindrical outer surfaces of the boreholes and the groundwater flows around them. Nonetheless, noting that the diameter of the boreholes is relatively small compared to the overall dimensions of the borehole field, a comparison of the numerical CVFEM-FVM predictions and the moving-finite-line-source analytical solution is provided in this section, as it provides a useful check or verification of the correct implementation of the numerical method.

A spatial superposition of the moving-finite-line-source analytical solutions gives the outer surface temperature of all six boreholes ($n = 1 - 6$):

$$\bar{T}_{b,k,n}(t) = T_g + \sum_{m=1}^{N_b} \sum_{j=1}^{N_{z,ac}} \frac{d_b}{2k_s} q''_{b,k_j,ac,m} f_{k,n,k_j,ac,m}(t) \quad (38)$$

$$f_{k,n,k_j,ac,m}(t) = \frac{1}{2\Delta z_k} \int_{1/\sqrt{4\alpha_{eff}t}}^{\infty} \frac{1}{s^2} I(z_{k_j,ac-1}, \Delta z_{k_j,ac}, z_{k-1}, \Delta z_k) \exp\left(-s^2 \left\{ \left(d_{n,m} \cos \beta_{n,m} - \frac{v_T}{4\alpha_{eff}s^2} \right)^2 + d_{n,m}^2 \sin^2 \beta_{n,m} \right\}\right) ds \quad (39)$$

$$\begin{aligned} I(z_{j-1}, \Delta z_j, z_{k-1}, \Delta z_k) = & \operatorname{erfint}\left(\left(z_{k-1} - z_{j-1} + \Delta z_k\right)s\right) - \operatorname{erfint}\left(\left(z_{k-1} - z_{j-1}\right)s\right) + \\ & \operatorname{erfint}\left(\left(z_{k-1} - z_{j-1} - \Delta z_j\right)s\right) - \operatorname{erfint}\left(\left(z_{k-1} - z_{j-1} + \Delta z_k - \Delta z_j\right)s\right) + \operatorname{erfint}\left(\left(z_{k-1} + z_{j-1} + \right. \right. \\ & \left. \left. \Delta z_k\right)s\right) - \operatorname{erfint}\left(\left(z_{k-1} + z_{j-1}\right)s\right) + \operatorname{erfint}\left(\left(z_{k-1} + z_{j-1} + \Delta z_j\right)s\right) - \operatorname{erfint}\left(\left(z_{k-1} + z_{j-1} + \right. \right. \\ & \left. \left. \Delta z_k + \Delta z_j\right)s\right) \end{aligned} \quad (40)$$

$$\operatorname{erfint}(x) = \int_0^x \operatorname{erf}(x') dx' = x \operatorname{erf}(x) - \frac{1}{\sqrt{\pi}} (1 - \exp(-x^2)) \quad (41)$$

In Eq. (39), $\alpha_{eff} = k_{eff}/(\rho c_p)_{eff}$ is the effective thermal diffusivity of the groundwater-saturated soil; $d_{n,m} = \sqrt{(x_{b,n} - x_{b,m})^2 + (y_{b,n} - y_{b,m})^2}$ is the axial distance between boreholes n and m (it is set to $d_{n,n} = d_b/2$ for $n = m$); $\beta_{n,m} = \operatorname{Arg}(x_{b,n} - x_{b,m} + i(y_{b,n} - y_{b,m}))$ is the angle between boreholes n and m relative to the direction of flow (it is set to $\beta_{n,n} = \pi/2$ for $n = m$); and $v_T = U_{\infty} \rho_w c_{p,w}/(\rho c_p)_{eff}$ is an effective heat transport velocity. Eqs. (38) to (41) were obtained using the method of Claesson and Javed (2011), as elaborated in Cimmino and Bernier (2014), rather than the simplified moving-finite-line-source solution proposed by Tye-Gingras and Gosselin (2014) based on the method of Lamarche and Beauchamp (2007).

The outer-surface dimensionless temperatures (perimeter-average for the numerical results; denoted here as θ_b) along the active length of the boreholes at $t^* = 395$ are shown in Figure 6. The maximum difference between the numerical and analytical results for θ_b at the bottom of the active portion of the boreholes at $t^* = 395$ is 5.16 % for $Pe_{d_b} = 0.1$; and at the mid-point of this portion, this maximum difference is 0.14 %. The time variations of the overall-average outer-surface dimensionless temperatures of the boreholes (denoted here as $\bar{\theta}_b$) are shown in Figure 7. The maximum difference between the numerical and analytical results for $\bar{\theta}_b$ at $t^* = 395$ is 0.23 % for $Pe_{d_b} = 0.01$; and it is 0.008 % for $Pe_{d_b} = 0.1$.

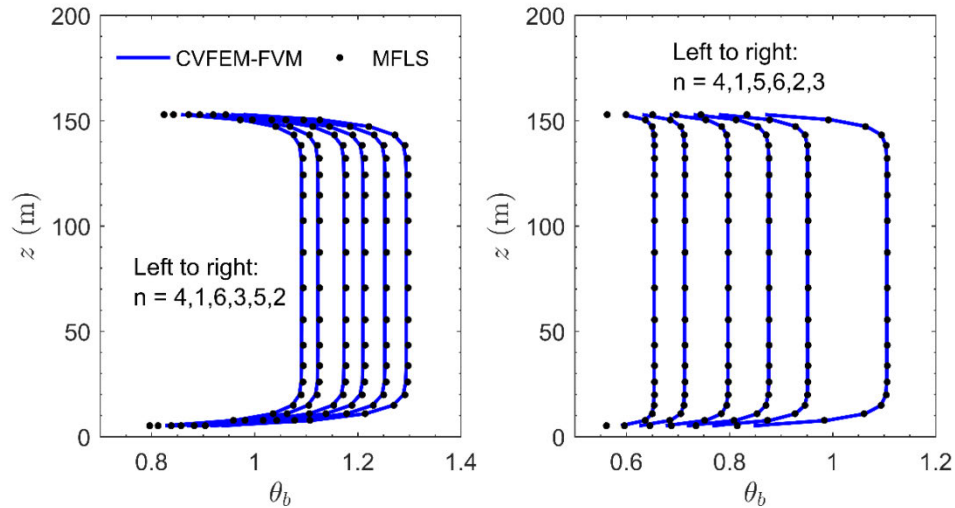


Figure 6. Comparison of the numerical and analytical results for the axial variation of the outer-surface dimensionless temperatures (perimeter-average for the numerical results; denoted here as θ_b) in a field of six boreholes at $t^* = 395$ for $Pe_{d_b} = 0.01$ (left) and $Pe_{d_b} = 0.1$ (right).

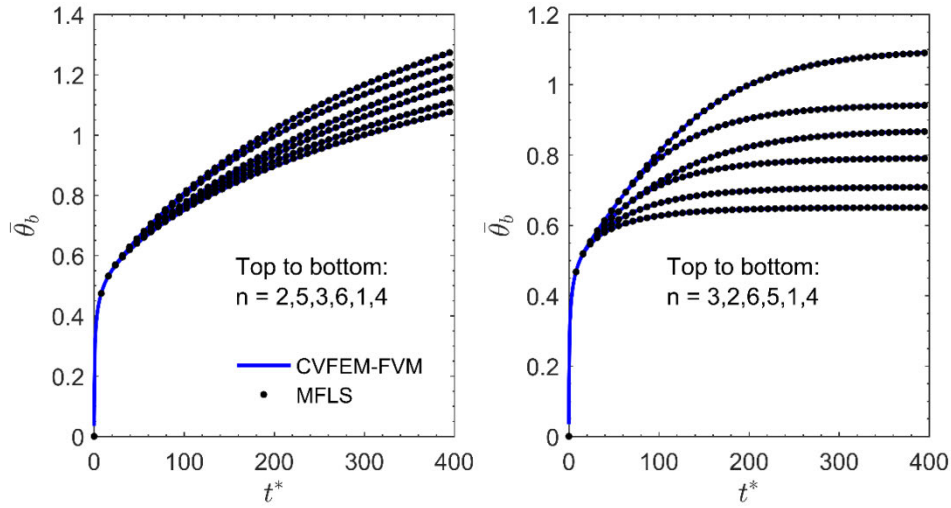


Figure 7. Comparison of the numerical and analytical results for the axial variation of the overall-average outer-surface temperatures (denoted here as $\bar{\theta}_b$) of the boreholes in a field of six boreholes at $t^* = 395$ for $Pe_{d_b} = 0.01$ (left) and $Pe_{d_b} = 0.1$ (right).

5.3. Two-year simulation of a 3 x 2 borehole field coupled to a ground-source heat-pump system

In this demonstration problem, the proposed hybrid numerical-semi-analytical method was used for a two-year simulation of a 3 x 2 borehole field (akin to that illustrated in Figs. 1 and 2) coupled to a ground-source heat-pump system. The geometry of the borehole field is the same as that considered in Section 5.2, which results in the same two-dimensional and three-dimensional grids. The input of time-varying total heat extraction rate was set equal to the heating and cooling loads obtained from a simulation of a small (5,000 sq-ft) office building using eQuest 3.65 [Hirsch (2016)]. This building was assumed to be equipped with a constant-efficiency heat pump. The building loads were calculated using ambient temperatures available in a representative January-to-December meteorological data file for Montreal, Canada.

Table 3. Input data used in the simulation of a 3 x 2 borehole field (akin to that illustrated in Figs. 1 and 2) coupled to a ground-source heat-pump system

Parameter	Units	Symbol	Value
Simulation time step	(min)	Δt	10
Maximum time	(years)	t_{max}	2
Number of boreholes	(-)	N_b	6
Bore field angle	(°)	β_b	30
Borehole length	(m)	H	150
Buried depth	(m)	D	4
Borehole spacing	(m)	B	5
Borehole diameter	(m)	d_b	0.15
U-tube pipe outer radius	(m)	$d_{p,o}$	0.042
U-tube pipe inner radius	(m)	$d_{p,i}$	0.034
Shank spacing	(m)	$d_{1-2}/2$	0.053
U-tube pipe inner-surface root-mean-square roughness	(m)	e_{rms}	1.5×10^{-6}
Undisturbed ground temperature	(°C)	T_g	13
Effective thermal conductivity	(W/m-K)	k_{eff}	2.5
Effective volumetric heat capacity	(J/m ³ K)	$(\rho c_p)_{eff}$	2.8×10^6
Groundwater volumetric heat capacity	(J/m ³ K)	$(\rho c_p)_w$	4.2×10^6
Groundwater regional Darcy velocity	(m/year)	U_∞	30
Groundwater dynamic viscosity	(Pa-s)	μ_w	1.3×10^{-3}
Soil porosity	(-)	ε	0.26
Soil permeability	(m ²)	K	2.5×10^{-13}
Grout thermal conductivity	(W/m-K)	k_g	1.5
U-tube pipe-wall thermal conductivity	(W/m-K)	k_p	0.4
Working-fluid thermal conductivity	(W/m-K)	k_f	0.45
Working-fluid dynamic viscosity	(Pa-s)	μ_f	4×10^{-3}
Working-fluid density	(kg/m ³)	ρ_f	1030
Working-fluid specific heat	(J/kg-K)	c_f	4000
Working-fluid mass flow rate per borehole	(kg/s)	\dot{m}_f	0.75

The other input data used in the simulation of the 3 x 2 borehole field are shown in Table 3. The soil properties are based on data for fine sand (see Table 1); the pipe-material properties correspond to those of HDPE pipes; and the working-fluid properties correspond to those of a 20% solution of propylene-glycol in water.

The total heat extraction rate (provided as an input) and the inlet and outlet working-fluid temperatures during the second year of the simulation year (calculated using the proposed hybrid method) are presented in Figs. 8 and 9, respectively. The maximum heat extraction rate is 75.6 kW and the maximum heat injection rate is 61.8 kW. The total heat extracted is 24870 kWh per year and the total heat injected is 25478 kWh per year. The minimum and maximum inlet working-fluid temperatures yielded by the simulation were -1.21°C and 28.26°C , respectively; and the minimum and maximum outlet fluid temperatures were 2.96°C and 24.85°C , respectively.

The predicted outlet working-fluid temperatures using the numerical model, and those obtained using a semi-analytical method based on a moving-finite-line-source solution of a simplified version of this problem, are presented in Fig. 9. This semi-analytical method uses the temporal superposition of the temperature step-response function to obtain the variation of the ground temperature at the borehole outer-surface and the semi-analytical method presented in Section 4.3 to obtain the outlet working-fluid temperature. The temperature step-response function is obtained from the method of Cimmino and Bernier (2014), using the moving-finite-line-source solution presented in Eq. (38). The temporal superposition is conducted using the method of Claesson and Javed (2012). During the second simulation year, the root-mean-square difference between the outlet working-fluid temperatures obtained from the numerical and semi-analytical models is 0.42°C . The maximum absolute difference is 2.04°C . In general, the semi-

analytical method underpredicts the temperature variations since heat is generated at the axis of the boreholes and thus the temperature at the borehole outer-surface responds slower to heat extraction.

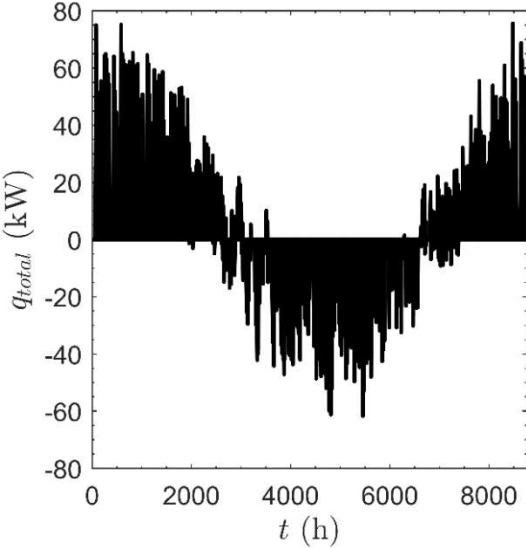


Figure 8. Yearly variation of the total heat extraction rate from the 3 x 2 borehole field.

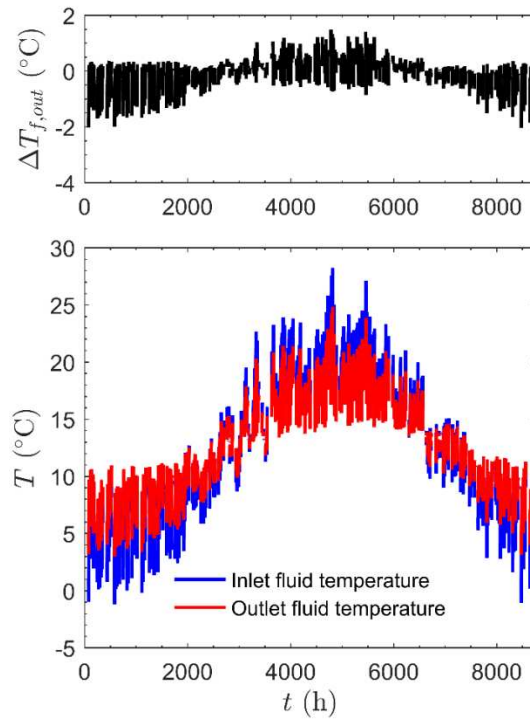


Figure 9. Difference between the outlet working-fluid temperature of the boreholes during the second simulation year (above); and inlet and outlet working-fluid temperatures during the second year of the simulation (below).

The temperature field in the groundwater saturated soil in the borehole field at the end of the second simulation year (December 31st) is presented in Figure 10 for a horizontal cross-section located at $z = D + H/2 = 79$ m. It shows that the minimum temperatures are located at the borehole outer-surfaces since the borehole field extracts heat from the soil at this time of the year. At the illustrated time, the overall average temperature at the borehole outer-surfaces is 12.13 °C. East of the boreholes, at $x \approx 20$ m, a temperature greater than T_g ($= 13^\circ\text{C}$) is observed. This maximum is caused by the heat injected into the ground earlier during the simulation year, and its location is shifted east of the boreholes due to advection by the groundwater. Soil temperatures downstream of the boreholes alternate between maximums and minimums due to

the yearly cycling of the building heating and cooling loads. In Fig. 10, the distance between maximum and minimum soil temperatures downstream of the boreholes is approximately equal to the half-year transport distance given by the effective heat transport velocity, $U_{\infty} \rho_w c_{p,w} / (\rho c_p)_{eff} \cdot 0.5 \text{ yr} = 22.5 \text{ m}$.

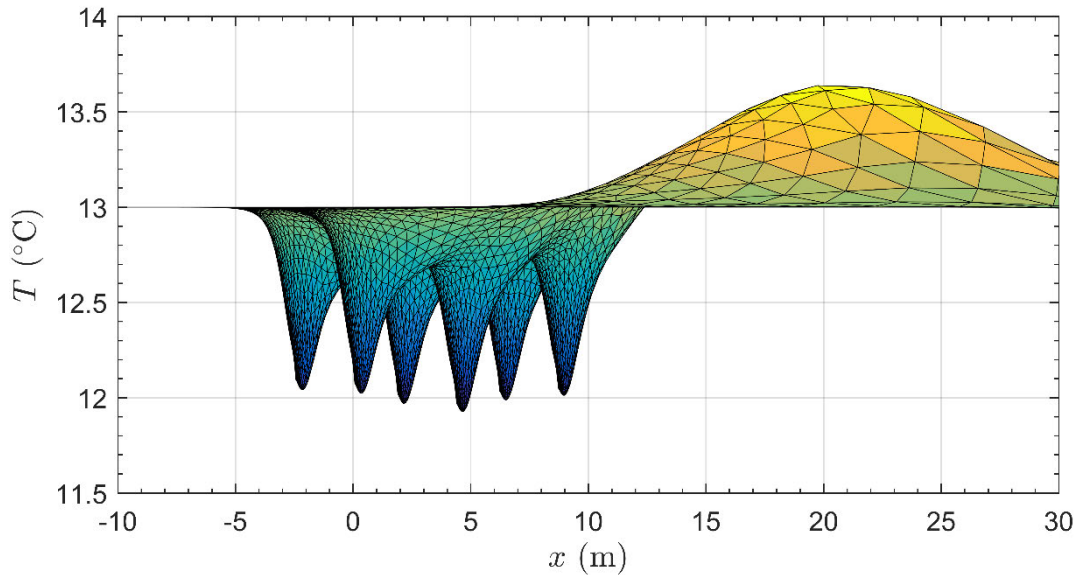


Figure 10. Groundwater-saturated soil temperatures in a horizontal cross-section of the borehole field located at $z = 79 \text{ m}$ at the end of the second simulation year.

6. Concluding remarks

The formulation, verification, and demonstration of a hybrid numerical-semi-analytical method for cost-effective simulations of the temperatures and heat transfer in borehole fields, in the presence of groundwater flow, were presented and discussed in the earlier sections of this paper.

In the proposed method, an amalgamation of a co-located control-volume finite element method and a finite volume method (CVFEM and FVM) [Baliga and Atabaki (2006); Lamoureux and Baliga (2011)] is used for solving the mathematical models of groundwater flow,

temperature, and heat transfer in the soil of the borehole field; and the bulk temperature distribution of the working fluid (flowing inside the legs of a U-tube pipe inserted inside each borehole and kept in place by grout) and the heat extraction (or addition) rates are obtained using a semi-analytical solution to a quasi-steady quasi-one-dimensional model. The numerical and semi-analytical solutions are iteratively coupled at each time step, using the conditions of no-slip, impermeability, equality of temperature, and continuity of heat flux at the interface between each borehole and the groundwater-saturated soil in the borehole field.

The hybrid numerical-semi-analytical method proposed in this paper follows the works of Bernier and Baliga (1992) and Lamoureux and Baliga (2015) who proposed cost-effective hybrid methods for computer simulations of closed-loop thermosyphons. It also complements and extends earlier hybrid methods for the investigation of heat transfer in borehole fields, such as those proposed by Li and Zheng (2009), Choi et al. (2013), for example, and others [see the review paper by Yang et al. (2010)].

The proposed hybrid numerical-semi-analytical method was successfully implemented and it produced encouraging results, some of which were presented and discussed in Section 5 of this paper. Potentially useful extensions of this method could be achieved by relaxing some of the assumptions on which it is based, as was discussed at the end of Subsection 3.1.

7. Acknowledgements

The following sources of financial support are gratefully acknowledged: a postdoctoral research scholarship awarded to the first author from the Fonds de recherche du Québec – Nature et Technologie (FRQNT); and an operating research grant awarded to the second author from the Natural Sciences and Engineering Research Council (NSERC) of Canada.

8. References

- Al-Khoury, R. and Focaccia, S. (2016), A spectral model for transient heat flow in a double U-tube geothermal heat pump system. *Renewable Energy*, **85**, 195-205.
- Baliga, B. R. and Atabaki, N. (2006), Control-volume-based finite-difference and finite-element methods. In W. J. Minkowycz, E. M. Sparrow, and J. Y. Murthy (Eds.), *Handbook of Numerical Heat Transfer*, 2nd Ed., John Wiley, New York, Chap. 6, 191-224.
- Baliga, B. R. and Lokhmanets, I. (2016), Generalized Richardson extrapolation procedures for estimating grid-independent numerical solutions. *International Journal of Numerical Methods for Heat & Fluid Flow*, **26**, pp. 1121-1144.
- Baliga, B. R., Lokhmanets, I., and Cimmino, M. (2017), Numerical methods for conduction-type phenomena, in *Handbook of Thermal Science and Engineering*, Kulacki, F.A. (Ed.), Springer International Publishing AG, Berlin, Germany (doi:10.1007/978-3-319-32003-8_4-1).
- Bauer, D., Heidemann, W., and Diersch, H.-J. G. (2011), Transient 3D analysis of borehole heat exchanger modeling. *Geothermics*, **40**, 250-260.
- Beier, R. A. (2014), Transient heat transfer in a U-tube borehole heat exchanger. *Applied Thermal Engineering*, **62**, 256-266.
- Belzile, P., Lamarche, L., and Rousse, D. (2016), Geothermal heat exchange in boreholes with independent sources. *Applied Thermal Engineering*, **98**, 1221-1230.
- Bernier, M. A. and Baliga, B. R. (1992), A 1-D/2-D model and experimental results for a closed-loop thermosyphon with vertical heat transfer sections. *International Journal of Heat and Mass Transfer*, **35**, 2969-2982.
- Carslaw, H. S. and Jaeger, J. C. (1959), *Conduction of heat in solids* (Vol. 2). Clarendon Press Oxford.
- Capozza, A., De Carli, M., and Zarrella, A. (2013), Investigations on the influence of aquifers on the ground temperature in ground-source heat pump operation. *Applied Energy*, **107**, 350-363.
- Chiasson, A. D., Rees, S. J., and Spitler, J. D. (2000), A preliminary assessment of the effects of groundwater flow on closed-loop ground source heat pump systems. *ASHRAE Transactions*, **106**, 380-393.

- Chiasson, A., and O'Connell, A. (2011), New analytical solution for sizing vertical borehole ground heat exchangers in environments with significant groundwater flow: Parameter estimation from thermal response test data. *HVAC and R Research*, **17**, 1000-1011.
- Choi, J. C., Park, J., and Lee, S. R. (2013), Numerical evaluation of the effects of groundwater flow on borehole heat exchanger arrays. *Renewable Energy*, **52**, 230-240.
- Cimmino, M., and Bernier, M. (2014), A semi-analytical method to generate g-functions for geothermal bore fields. *International Journal of Heat and Mass Transfer*, **70**, 641-650.
- Cimmino, M. (2016), Fluid and borehole wall temperature profiles in vertical geothermal boreholes with multiple U-tubes. *Renewable Energy*, **96**, 137-147.
- Claesson, J. and Hellström, G. (2011), Multipole method to calculate borehole thermal resistances in a borehole heat exchanger. *HVAC&R Research*, **17**, 895-911.
- Claesson, J. and Javed, S. (2011), An analytical method to calculate borehole fluid temperatures for time-scales from minutes to decades. *ASHRAE Transactions*, **117**, 279-288.
- Claesson, J. and Javed, S. (2012), A load-aggregation method to calculate extraction temperatures of borehole heat exchangers. *ASHRAE Transactions*, **118**, 530-539.
- Cotta, R. M. and Mikhailov, M. D. (2006), Hybrid methods and symbolic computations. In Minkowycz, W. J., Sparrow, E. M., and Murthy, J. Y. (Eds.), *Handbook of Numerical Heat Transfer*, 2nd Ed., John Wiley, New York, Chapter 16, 493-522.
- Dai, L. H., Shang, Y., Li, X. L., and Li, S. F. (2016), Analysis on the transient heat transfer process inside and outside the borehole for a vertical U-tube ground heat exchanger under short-term heat storage. *Renewable Energy*, **87**, 1121-1129.
- Diao, N., Li, Q., and Fang, Z. (2004), Heat transfer in ground heat exchangers with groundwater advection. *International Journal of Thermal Sciences*, **43**, 1203-1211.
- Diersch, H. J. G., Bauer, D., Heidemann, W., Rühak, W., and Schätzl, P. (2011a), Finite element modeling of borehole heat exchanger systems: Part 1. Fundamentals. *Computers & Geosciences*, **37**, 1122-1135.
- Diersch, H. J. G., Bauer, D., Heidemann, W., Rühak, W., and Schätzl, P. (2011b), Finite element modeling of borehole heat exchanger systems: Part 2. Numerical simulation. *Computers & Geosciences*, **37**, 1136-1147.

- Erol, S., Hashemi, M. A., and François, B. (2015), Analytical solution of discontinuous heat extraction for sustainability and recovery aspects of borehole heat exchangers. *International Journal of Thermal Sciences*, **88**, 47-58.
- Eskilson, P. (1987), Thermal analysis of heat extraction boreholes. Ph.D. thesis, University of Lund, Lund, Sweden.
- Eskilson, P. and Claesson, J. (1988), Simulation model for thermally interacting heat extraction boreholes. *Numerical Heat Transfer*, **13**, 149-165.
- Eslami-Nejad, P. and Bernier, M. (2011). Coupling of geothermal heat pumps with thermal solar collectors using double U-tube boreholes with two independent circuits. *Applied Thermal Engineering*, **31**, 3066-3077.
- Fan, R., Jiang, Y., Yao, Y., Shiming, D., and Ma, Z. (2007). A study on the performance of a geothermal heat exchanger under coupled heat conduction and groundwater advection. *Energy*, **32**, 2199-2209.
- Gehlin, S. E. A. and Hellström, G. (2003), Influence on thermal response test by groundwater flow in vertical fractures in hard rock. *Renewable Energy*, **28**, 2221-2238.
- Ghoreishi-Madiseh, S. A., Hassani, F. P., Mohammadian, A., and Radziszewski, P. H. (2013), A transient natural convection heat transfer model for geothermal borehole heat exchangers. *Journal of Renewable and Sustainable Energy*, **5**, 043104.
- Hecht-Méndez, J., Molina-Giraldo, N., Blum, P., and Bayer, P. (2010), Evaluating MT3DMS for Heat Transport Simulation of Closed Geothermal Systems. *Ground Water*, **48**, 741-756.
- Hecht-Méndez, J., de Paly, M., Beck, M., and Bayer, P. (2013), Optimization of energy extraction for vertical closed-loop geothermal systems considering groundwater flow. *Energy Conversion and Management*, **66**, 1-10.
- Hellström, G. (1991), Ground heat storage. Thermal Analyses of Duct Storage Systems I: Theory. Ph.D. thesis, University of Lund, Lund, Sweden.
- Hidalgo, J. J., Carrera, J., and Dentz, M. (2009), Steady state heat transport in 3D heterogeneous porous media. *Advances in Water Resources*, **32**, 1206-1212.
- Hirsch, J. J. (2016), *eQUEST: Quick Energy Simulation Tool*.
- Hsu, C. T. and Cheng, P. (1990), Thermal dispersion in a porous medium. *International Journal of Heat and Mass Transfer*, **33**, 1587-1597.

- Incropera, F. P. and DeWitt, D. P. (2002), *Fundamentals of Heat and Mass Transfer*, 5th Ed. John Wiley and Sons, New York.
- Javed, S. and Spitler, J. (2017), Accuracy of borehole thermal resistance calculation methods for grouted single U-tube ground heat exchangers. *Applied Energy*, **187**, 790-806.
- Kavanaugh, S. and Rafferty, K. (2014), *Geothermal heating and cooling: Design of ground-source heat pump systems*. American Society of Heating, Refrigerating, and Air-Conditioning (ASHRAE book), Atlanta, Georgia, U.S.A.
- Lamarche, L. and Beauchamp, B. (2007), A new contribution to the finite line-source model for geothermal boreholes. *Energy and Buildings*, **39**, 188-198.
- Lamoureux, A. and Baliga, B. R. (2011), Improved formulations of the discretized pressure equation and boundary treatments in co-located equal-order control-volume finite-element methods for incompressible fluid flow. *Numerical Heat Transfer, Part B: Fundamentals*, **59**, 442-472.
- Lamoureux, A. and Baliga, B. R. (2015), Hybrid numerical methods combining discretized multidimensional and segmented-quasi-one-dimensional models for simulating thermofluid systems. *International Journal of Numerical Methods for Heat & Fluid Flow*, **25**, 1404-1425.
- Lee, C. K., and Lam, H. N. (2012), A modified multi-ground-layer model for borehole ground heat exchangers with an inhomogeneous groundwater flow. *Energy*, **47**, 378-387.
- Li, M. and Lai, A. C. K. (2015), Review of analytical models for heat transfer by vertical ground heat exchangers (GHEs): A perspective of time and space scales. *Applied Energy*, **151**, 178-191.
- Li, Z. and Zheng, M. (2009), Development of a numerical model for the simulation of vertical U-tube ground heat exchangers. *Applied Thermal Engineering*, **20**, 920-924.
- Metzger, T., Didierjean, S., and Maillet, D. (2004), Optimal experimental estimation of thermal dispersion coefficients in porous media. *International Journal of Heat and Mass Transfer*, **47**, 3341-3353.
- Molina-Giraldo, N., Bayer, P., and Blum, P. (2011a), Evaluating the influence of thermal dispersion on temperature plumes from geothermal systems using analytical solutions. *International Journal of Thermal Sciences*, **50**, 1223-1231.

- Molina-Giraldo, N., Blum, P., Zhu, K., Bayer, P., and Fang, Z. (2011b), A moving finite line source model to simulate borehole heat exchangers with groundwater advection. *International Journal of Thermal Sciences*, **50**, 2506-2513.
- Nield, D. A. and Bejan, A. (2013), *Convection in porous media* (4th ed.). Springer, New York.
- Patankar, S. V. (1980), *Numerical heat transfer and fluid flow*. Hemisphere, Washington D.C.
- Pasquier, P. and Marcotte, D. (2012), Short-term simulation of ground heat exchanger with an improved TRCM. *Renewable Energy*, **46**, 92-99.
- Persson, P. O., and Strang, G. (2004). A simple mesh generator in MATLAB. *SIAM review*, **46**, 329-345.
- Raymond, J., Therrien, R., Gosselin, L., and Lefebvre, R. (2011), Numerical analysis of thermal response tests with a groundwater flow and heat transfer model. *Renewable Energy*, **36**, 315-324.
- Rhie, C. M. and Chow, W. L. (1983), Numerical study of the turbulent flow past an airfoil with trailing edge separation. *AIAA Journal*, **21**, 1525-1532.
- Rivera, J. A., Blum, P., and Bayer, P. (2015), Analytical simulation of groundwater flow and land surface effects on thermal plumes of borehole heat exchangers. *Applied Energy*, **146**, 421-433.
- Rottmayer, S. P., Beckman, W. A., and Mitchell, J. W. (1997). Simulation of a single vertical U-tube ground heat exchanger in an infinite medium, *ASHRAE Transactions*, **103**, 651-659.
- Rouleau, J., and Gosselin, L. (2016), Inverse heat transfer applied to a hydrogeological and thermal response test for geothermal applications. *International Journal of Thermal Sciences*, **109**, 70-80.
- Rouleau, J., Gosselin, L., and Raymond, J. (2016), New concept of combined hydro-thermal response tests (H/TRTS) for ground heat exchangers. *Geothermics*, **62**, 103-114.
- Saad, Y. (2003). *Iterative Methods for Sparse Linear Systems* (2nd ed.). Society for Industrial and Applied Mathematics (SIAM), Philadelphia, U.S.A.
- Spitler, J. D. (2005), Editorial: Ground-source heat pump system research – Past, present, and future. *HVAC&R Research*, **11**, 165-167.
- Sutton, M. G., Nutter, D. W., and Couvillion, R. J. (2003), A Ground Resistance for Vertical Bore Heat Exchangers With Groundwater Flow. *Journal of Energy Resources Technology*, **125**, 183-189.

- Therrien, R., McLaren, R., Sudicky, E., and Panday, S. (2010), HydroGeoSphere: A three-dimensional numerical model describing fully-integrated subsurface and surface flow and solute transport. *Groundwater Simulations Group, University of Waterloo, Waterloo, ON.*
- Thevenin, J. and Sadaoui, D. (1995), About enhancement of heat transfer over a circular cylinder embedded in a porous medium. *International communications in heat and mass transfer*, **22**, 295-304.
- Tye-Gingras, M. and Gosselin, L. (2014), Generic ground response functions for ground exchangers in the presence of groundwater flow. *Renewable Energy*, **72**, 354-366.
- Vafai, K. (2005), *Handbook of porous media*. Taylor and Francis, Boca Raton, Florida.
- Vafai, K. and Tien, C. L. (1981), Boundary and inertia effects on flow and heat transfer in porous media. *International Journal of Heat and Mass Transfer*, **24**, 195-203.
- Wagner, V., Blum, P., Kübert, M., and Bayer, J. (2013), Analytical approach to groundwater-influenced thermal response tests of grouted borehole heat exchangers. *Geothermics*, **46**, 22-31.
- Wang, H., Qi, C., Du, H., and Gu, J. (2009), Thermal performance of borehole heat exchanger under groundwater flow: A case study from Baoding. *Energy and Buildings*, **41**, 1368-1373.
- Yang, H., Cui, P., and Fang, Z. (2010), Vertical-borehole ground-coupled heat pumps: A review of models and systems. *Applied Energy*, **87**, 16-27.
- Yavuzturk, C., Spitler, J. D., and Rees, S. J. (1999), A transient two-dimensional finite volume model for the simulation of vertical U-tube ground heat exchangers, *ASHRAE Transactions*, **105** (1999), 465-474.
- Zanchini, E., Lazzari, S., and Priarone, A. (2012), Long-term performance of large borehole heat exchanger fields with unbalanced seasonal loads and groundwater flow. *Energy*, **38**, 66-77.
- Zeng, H., Diao, N., and Fang, Z. (2003), Heat transfer analysis of boreholes in vertical ground heat exchangers. *International Journal of Heat and Mass Transfer*, **46**, 4467-4481.
- Zhang, W., Yang, H., Guo, X., Yu, M., and Fang, Z. (2016), Investigation on groundwater velocity based on the finite line heat source seepage model. *International Journal of Heat and Mass Transfer*, **99**, 391-401.

Zhao, J., Wang, H., Li, X., and Dai, C. (2008), Experimental investigation and theoretical model of heat transfer of saturated soil around coaxial ground coupled heat exchanger. *Applied Thermal Engineering*, **28**, 116-125.